RADC-TR-82-91
Final Technical Report
May 1982

SIMULATION OF GROUND-TO-SPACE OPTICAL PROPAGATION

Hughes Research Laboratories

Sponsored by
Defense Advanced Research Projects Agency (DOD)
ARPA Order No. 4021

APPROVED FOR PUBLIC RELEASE; DISTRIBUTION UNLIMITED

ROME AIR DEVELOPMENT CENTER
Air Force Systems Command
Griffiss Air Force Base, NY 13441

This report has been reviewed by the RADC Public Affairs Office (PA) and is releasable to the National Technical Information Service (NTIS). At NTIS it will be releasable to the general public, including foreign nations.

RADC-TR-82-91 has been reviewed and is approved for publication.

APPROVED: Patrick J. Martone

PATRICK J. MARTONE, Captain, USAF
Project Engineer

APPROVED:

LOUIS E. WHITE, Lt Colonel, USAF
Acting Chief, Surveillance Division

FOR THE COMMANDER: John P. Huss

JOHN P. HUSS
Acting Chief, Plans Office

If your address has changed or if you wish to be removed from the RADC mailing list, or if the addressee is no longer employed by your organization, please notify RADC (OCSE) Griffiss AFB NY 13441. This will assist us in maintaining a current mailing list.

Do not return copies of this report unless contractual obligations or notices on a specific document requires that it be returned.

SIMULATION OF GROUND-TO-SPACE OPTICAL PROPAGATION

W. P. Brown
S. C. Fry
G. C. Valley

Contractor: Hughes Research Laboratories
Contract Number: F30602-80-C-0297
Effective Date of Contract: 15 September 1980
Contract Expiration Date: 15 September 1981
Short Title of Work: Simulation of Ground-to-Space Optical Propagation
Program Code Number: 0E20
Period of Work Covered: Sep 80 - Sep 81

Principal Investigator: Dr. W. Brown
Phone: (213) 456-6411

Project Engineer: Capt. P.J. Martone
Phone: (315) 330-3145

This research was supported by the Defense Advanced Research Projects Agency of the Department of Defense and was monitored by Captain Patrick Martone (OCSF), Griffiss AFB NY 13441 under Contract F30602-80-C-0297.

UNCLASSIFIED

SECURITY CLASSIFICATION OF THIS PAGE (When Data Entered)

REPORT DOCUMENTATION PAGE		READ INSTRUCTIONS BEFORE COMPLETING FORM
1. REPORT NUMBER RADC-TR-82-91	2. GOVT ACCESSION NO.	3. RECIPIENT'S CATALOG NUMBER
4. TITLE (and Subtitle) SIMULATION OF GROUND-TO-SPACE OPTICAL PROPAGATION		5. TYPE OF REPORT & PERIOD COVERED Final Technical Report 15 Sep 80 - 15 Sep 81
		6. PERFORMING ORG. REPORT NUMBER N/A
7. AUTHOR(s) W. P. Brown S. C. Fry G. C. Valley		8. CONTRACT OR GRANT NUMBER(s) F30602-80-C-0297
9. PERFORMING ORGANIZATION NAME AND ADDRESS Hughes Research Laboratories 3011 Malibu Canyon Road Malibu CA 90265		10. PROGRAM ELEMENT PROJECT, TASK AREA & WORK UNIT NUMBERS 62301E D0210000
11. CONTROLLING OFFICE NAME AND ADDRESS Defense Advanced Research Projects Agency 1400 Wilson Blvd Arlington VA 22209		12. REPORT DATE May 1982 13. NUMBER OF PAGES 94
14. MONITORING AGENCY NAME & ADDRESS (if different from Controlling Office) Rome Air Development Center (OCSE) Griffiss AFB NY 13441		15. SECURITY CLASS. (of this report) UNCLASSIFIED 15a. DECLASSIFICATION/DOWNGRADING SCHEDULE N/A

16. DISTRIBUTION STATEMENT (of this Report)

Approved for public release; distribution unlimited.

17. DISTRIBUTION STATEMENT (of the abstract entered in Block 20, if different from Report)

Same

18. SUPPLEMENTARY NOTES

RADC Project Engineer: Patrick J. Martone, Captain, USAF (OCSE)

19. KEY WORDS (Continue on reverse side if necessary and identify by block number)

SLC	Simulation
Uplink	Anisoplanatism
Adaptive-Optics	Propagation

20. ABSTRACT (Continue on reverse side if necessary and identify by block number)

This work was performed in support of the Strategic Laser Communication (SLC) Uplink program. Computer simulations were performed to determine the degree of correction achievable with phase-conjugate adaption optics. The purpose of the computer simulations was to investigate the effect of four error sources on the performance of an adaptive optics system used to compensate for the effects of atmospheric turbulence on the propagation of visible wavelength laser radiation between a ground-based

DD FORM 1 JAN 73 1473 EDITION OF 1 NOV 65 IS OBSOLETE

UNCLASSIFIED

SECURITY CLASSIFICATION OF THIS PAGE (When Data Entered)

transmitter and a space-borne receiver. The four error sources considered in this work were: (1) finite spatial bandwidth corrector mirror; (2) finite temporal bandwidth servo system; (3) measurement noise; and (4) anisoplanatism. We investigated both the separate and combined effects of these errors. The results obtained when the errors were introduced separately agree well with the predictions obtained from the analytical relations used to represent these effects in the SLC Uplink model prepared by RADC for use in systems calculations. As expected, we found that when all of the errors are present simultaneously their effects are not always accurately modeled by these analytical relations. This is particularly true in the case of the effects of having finite spatial and/or temporal bandwidth in combination with those due to anisoplanatism. In such cases, the Strehl ratio obtained in the simulations was up to a factor of two higher than that predicted by the SLC Uplink model analytical relations. Calculations pertaining to the application of optimal estimation techniques to improve adaptive optics performance in the presence of anisoplanatism were also performed.

TABLE OF CONTENTS

LIST OF ILLUSTRATIONS

LIST OF TABLES

I. INTRODUCTION AND SUMMARY

1.1 Background

The work on this contract was performed in support of the Strategic Laser Communication (SLC) Uplink program, which concerns the propagation of a visible wavelength laser beam from a ground station to a relay satellite located in a synchronous orbit. In order to transfer the laser energy efficiently to the relay it will be necessary to employ an adaptive-optics system to compensate for the effect of atmospheric turbulence. This can be appreciated by noting that the Airy disk of a diffraction limited 4 meter ground-based telescope is approximately 10 meters in extent at synchronous altitude ... the maximum convenient size of a spaceborne relay mirror. Yet, without correction, visible radiation from a ground-based 4 meter telescope would be spread over a region approximately 400 meters in extent (assuming a 10 cm. phase coherence length). There are a number of factors that will affect the degree to which an adaptive-optics system can correct for the effects of atmospheric turbulence. The most important of these are: (1) the spatial frequency response of the corrector mirror; (2) the temporal response of the adaptive system; (3) the signal-to-noise ratio of the correction system; and (4) the effects of anisoplanatic errors (those errors caused by a

displacement of the propagation paths taken by the transmitted and reference waves ... originating from the point-ahead requirement associated with the finite time it takes the radiation to travel to the relay and back and/or station-keeping errors in the position of a separate satellite used to carry the reference.

Analytical techniques are available for estimating the effect of each of the above errors taken separately. The combined effect of all the errors is usually accounted for by multiplying the Strehl ratios associated with the separate errors. This approach is based on the concept that each of the error sources contributes independently to the overall system phase error. The total mean square value of this error is assumed equal to the sum of the mean square fluctuations of the individual contributions. It has been appreciated for some time that the independence assumption on which this approach is based is, strictly speaking, not valid; and thus, that the overall Strehl ratios predicted by such a technique may be unduly pessimistic. There are two ways in which to avoid this problem. Either we modify the analysis to account for the error dependencies or we do a detailed simulation of the propagation and adaptive optics with the dependencies included. At the time the work on this contract was originally contemplated the required analytical modifications were not available.[1] Thus, we proposed to study this problem using a numerical simulation

approach based on the Hughes Research Laboratories (HRL) propagation and adaptive optics software, which includes an accurate modeling of the error dependency effects. The capabilities of this software are described in section II.

1.2 Summary of Results

Before proceeding with the simulation studies we had to modify the software in several ways. One of the most significant changes in terms of the effort required was the modification of the software to accommodate operation on the Cray-1 computer rather than the CDC 7600 computer for which the software was originally written. This was necessitated by the fact that: (1) the simulation requires a large high-speed scientific computer such as the CDC 7600 or the Cray-1; (2) for reasons of economy and past experience we wished to use the computers located at the Air Force Weapons Laboratory (AFWL); and (3) the AFWL computer center replaced their CDC 7600 computers with a Cray-1 shortly before the start of the contract. Other software modifications and upgrades included increasing the size of the propagation mesh to enable the simulation of larger size transmitter optics, modifying the manner in which the random medium is generated and stored, increasing the number of sub-apertures into which the adaptive-optics receiver can be divided, and modifying the algorithm used to estimate actuator positions from wavefront slope data. The nature of these modifications is discussed in more detail in section III.

One of the most important consequences of the modifications is that, as a result of changes in the manner in which the turbulent medium is stored (on disk rather than in random access memory), we are now able to perform the propagation calculations on a mesh having up to 256 x 256 points. Before these changes we were limited to a 64 x 64 point mesh. The extended resolution capability provided by this modification is especially important in the simulation of the effects of anisoplanatism. We found that a 256 x 256 mesh was required to obtain adequate accuracy in these calculations. Small scale inhomogeneities apparently play an important role in these effects.

The propagation software is capable of modeling the effects of thermal blooming along with those caused by linear absorption, scattering and turbulence. Thus, we performed a limited set of runs to determine the relative importance of thermal blooming in the SLC Uplink propagation. These studies revealed that thermal blooming will not significantly distort the propagated energy at the power levels contemplated in this application. For example, the Strehl ratio due to thermal blooming was found to be .97 at a 30 kw power level, under the assumption that the wind velocity has the relatively conservative altitude profile shown in Figure 4. Since these effects are small and their

inclusion complicates the simulation and the interpretation of the results, we neglected them in the simulations performed to determine the SLC Uplink system performance.

In order to ascertain whether or not the simulation produces results that agree with the analytical theories in the case where there is no dependency among the various errors, we performed a set of simulations in which only one of the errors was present; e.g., a system having a finite actuator mirror but infinite temporal bandwidth and signal-to-noise ratio and no anisoplanatic error, and so forth. In the case of the noise simulations,however, we utilized a finite actuator mirror since it does not make sense to have infinite spatial frequency response in this case (an infinite actuator mirror would have a signal-to-noise ratio of zero since the sub-aperture size would then be infinitesimally small). In all of the cases in which the errors were independent, we obtained simulation results that agree well with the theoretical predictions (the noise effects are easily corrected for the effects of having a finite spatial frequency deformable mirror since these effects are essentially independent in any case). This agreement gives us confidence that the simulation has no major bugs and thus can be relied on to yield accurate results in cases where the analytical theories do not apply. It should be noted that the agreement between the computer and theoretical results in these cases indicates that the

effects of diffraction are not terribly important in the SLC propagation problem. This follows from the fact that the theoretical predictions for the separate effects can be derived solely on the basis of geometrical optical considerations. The predictions can be derived by considering the difference between the phase correction introduced by the adaptive-optics system and the geometrical optics phase associated with the path taken by the transmitted wave. This simplifies the analysis of the effect of errors and provides the basis of a more detailed analytical modeling of the combined effects of the errors recently initiated at Hughes under internal funds.[2]

Two types of simulations were performed in which the effects of error dependency were included. First, we studied the effect of anisoplanatic errors on an adaptive system that has a finite spatial bandwidth mirror but otherwise is perfect; i.e., has infinite temporal bandwidth and signal-to-noise ratio. These studies showed that the effects of error dependency can significantly affect the system Strehl ratio. For example, we found that the Strehl ratio is 50% to 100% higher than the theory predicts in the case of a system having a 1 meter aperture, a deformable corrector mirror with 50 to 350 actuators, and a reference beacon offset 20 μrad. from the point-ahead direction. The largest discrepancy between the theoretical predictions and the computer results occurs for the system having the lowest

spatial frequency response. This implies that the spatial frequencies of the errors associated with the anisoplanatic effect extend down at least to the cutoff point for a 50 actuator mirror. The phase correction introduced by a finite actuator mirror does not contain spatial frequencies above its cutoff and therefore it is not appropriate to include these spatial frequencies in those associated with the anisoplanatic effect. It is apparent that the same type of consideration applies in the more general case where all of the errors are present simultaneously ... errors should be counted only once. If the phase correction introduced by the adaptive-optics system does not contain spatial frequencies beyond a cutoff point, due to the spatial and temporal frequency limitations of the system, the anisoplanatic effect will not contain these errors. Even in cases where there is no anisoplanatism, a dependency still exists between the spatial and temporal errors since there is a correlation between the spatial and temporal variation of the atmospheric phase error.This is caused by the fact that the higher temporal frequency errors tend to be associated with the higher spatial frequency errors (Taylor's "frozen turbulence" hypothesis[3]).

The modeling in the above simulations was simplified by virtue of the neglect of the effects of finite temporal bandwidth and noise. This allowed us to utilize a "local loop" type of modeling in which it is not necessary to

update the propagation information every servo time increment. Rather, we propagate the reference wave to the receiver and use this field for all time increments. A complete modeling of the closed-loop operation of the adaptive system servo is performed including the behavior of the wavefront sensor, optimal estimator and deformable mirror combination, but the system temporal bandwidth is effectively infinite since the error is time independent. After the servo has converged, we then introduce the phase correction and propagate the corrected wave to the relay satellite. Since only a limited number of propagation calculations are required in this type of simulation, it is considerably less expensive than the more general simulations in which the effects of temporal bandwidth and noise are included.

Because of the expense, only a limited number of simulations were performed in which all of the four error sources were included. We concentrated on cases for which the results might have some practical significance to the SLC Uplink program in addition to providing an indication of the importance of the error dependency effects. We simulated three different adaptive-optics systems which illustrate the impact of anisoplanatism on the degree of correction obtainable. In these simulations we utilized a canonical adaptive-optics system having a 1 meter corrector mirror with 346 actuators, a 100 Hz servo bandwidth,and a

wavefront sensor signal-to-noise ratio of 7. Based on the previous simulation results and the theoretical scaling relations, such a system should yield a nearly diffraction limited compensation in the absence of anisoplanatism. Results were obtained for systems in which the reference was offset from the point-ahead direction by 20, 5, 0 μrad. (20 μrad. corresponding to a system for which the reference beacon is located on the relay satellite; 5 μrad. to a system for which the station keeping accuracy of the beacon satellite is 5 μrad., and 0 μrad. to a system having a perfectly positioned beacon satellite ... i.e., no anisoplanatic errors). In the case in which the offset was 20 μrad., the Strehl ratio obtained from the computer simulation was 50% higher than that predicted by the simple theories. This is the same discrepancy that was obtained in the above simulations in which the temporal bandwidth and noise errors were zero. This implies that the 100 Hz. bandwidth and the signal-to-noise ratio of 7 used in the simulations are sufficiently high that the finite spatial frequency response of the mirror was the principal source of error dependency. Of course, had we simulated a system with a substantially lower temporal bandwidth, the discrepancy between the simulation results and the theoretical predictions would undoubtedly been larger. In the case in which the offset was 5 μrad., the Strehl obtained from the simulation was 20% higher than that

predicted by theory; and at zero offset it was 10% higher (which is,principally, a measure of the dependency between the errors associated with the finite spatial and temporal bandwidth of the system).

Perhaps the most important result of the simulations studies is the observation that the amount of fluctuation in the corrected Strehl ratio is strongly dependent on the degree of correction. The magnitude of the fluctuations increases as the fidelity of the correction is reduced. The uncorrected irradiance at the relay satellite fluctuates more than 100% about the mean; whereas, the irradiance obtained from an adaptive system yielding a mean Strehl greater than .7 typically fluctuates less than 10%. The reduction in performance associated with the average Strehl ratio is thus not indicative of the true price paid for using a less capable system. In addition, the irradiance at the relay mirror fluctuates about the mean ... occasionally suffering deep fades. The simulation software provides an effective way of delineating the importance of this phenomenon as a function of the system parameters. A detailed study of the statistics of the fading, however, will require a simplified propagation model since such information inherently requires that large amounts of data be processed.

In addition to the code modification and computer simulation work we also investigated the effect of optimal estimation on the magnitude of the errors associated with the anisoplanatic effect. When the angular offset of the reference beam from the point-ahead direction is very large, it is obvious that the best policy is to disregard the phase information provided by the reference altogether since it is uncorrelated with the phase errors introduced on the path taken by the transmitted wave. Optimal estimation provides a means of determining the optimum correction policy in the intermediate cases between the limits where there is no anisoplanatic error and the extreme case mentioned above where there is no correlation between the measured phase and the desired correction. Hanson[4] has derived an optimal estimation procedure that is based on the assumption that the temporal and angular dependence of the phase error are linearly related. With this assumption it is theoretically possible to reduce the anisoplanatic error by appropriate processing of a set of temporal phase measurements combined with a knowledge of the statistical properties of the atmospheric phase errors. Unfortunately, this approach does not work in the SLC Uplink situation since the assumption of a linear dependence between the temporal and angular dependence of the phase error is not valid for a synchronous satellite (the linear dependence requires that the turbulent eddies transit the beam with a velocity that increases

linearly with altitude ... e.g., by virtue of a large angular velocity associated with the satellite motion). We have developed an alternative optimal estimation procedure that does not rely on this assumption. Instead, it utilizes the information available from a set of instantaneous phase measurements obtained from the various sub-apertures into which the transmitter aperture is divided by the wavefront sensor. In this approach, as in that used by Hanson, the statistical correlation properties of the atmosphere are assumed known.

The degree to which the effects of anisoplanatism can be mitigated by optimal estimation techniques depends primarily on the magnitude of the angular offset from the point-ahead direction, the signal-to-noise ratio, and the spatial and temporal bandwidth of the adaptive-optics system. As indicated above, the optimal policy for large angular offsets is no correction at all. This is clearly not an acceptable solution for the SLC Uplink system since we cannot tolerate the severe reduction and fluctuation of irradiance intercepted by the relay mirror under these conditions. Thus, it is apparent that we will be operating with a small angular offset from the point-ahead direction ... caused,for example, by station-keeping errors. Based on the work of Hanson and the simulation data performed on this contract, it would seem that angular offsets of the order of 5 to 10 μrad. or less will be required in order

to have a chance of substantially improving the system performance via optimal estimation. There is also evidence that the optimal estimation results will strongly depend on the system signal-to-noise ratio. Finally, the simulation results and the phase error correlation studies discussed in Appendix A strongly suggest that much of the improvement predicted by the optimal estimation theories will disappear when the finite spatial and temporal bandwidth of the adaptive-optics system is taken into account. Contrary to the conclusions reached by Hanson, our simulation studies indicate that the anisoplanatic effect is strongly dependent on the small scale phase fluctuations. This was illustrated by the sensitivity of the anisoplanatic simulations to the number of mesh points used in the simulations (the results obtained with a 128 x 128 mesh did not agree with those obtained with a 256 x 256 mesh); and to small displacements of the correction phase along the direction of the satellite motion (a 1 cm. displacement produces significant changes in the anisoplanatic effect). Moreover, the work in Appendix A shows that the low-order phase aberrations such as tilt, focus, coma, astigmatism, ... etc., are correlated over offset angles that are much larger than the isoplanatic angle predicted by the theory and calculated in the simulations. Unfortunately, error dependency is a double-edged sword. Just as it is not correct to count dependent errors more than once, it also is not correct to

count on a significant improvement in system performance via optimal estimation if our system does not sense the small scale errors contributing most significantly to this (theoretical maximum) improvement.

II. HRL PROPAGATION AND ADAPTIVE-OPTICS SOFTWARE

The HRL software includes a detailed time-dependent propagation code based on a full-diffraction calculation of the propagation along atmospheric slant paths and a detailed modeling of the adaptive optics wavefront sensor and servo system. A brief description of this software is given in the following paragraphs. Those interested in a more complete discussion are referred to references 5 and 6.

2.1 Propagation modeling

The general features of the propagation modeling are shown in Figure 1. The atmosphere is represented by a layer extending 20 to 30 km. above the surface of the earth. Within this region we account for the effects of absorption, scattering, and medium inhomogeneities associated with turbulence; including their variation with altitude. The region above the atmosphere is assumed to be a vacuum. Propagation along paths inclined at an arbitrary angle to the zenith is modeled, which allows us to simulate propagation along the most general ground station to satellite path. The propagation within the atmosphere is simulated by a multi-step calculation in which the wave is propagated in a sequence of ten steps to the top of the atmosphere (which was assumed located at 20 km. in these

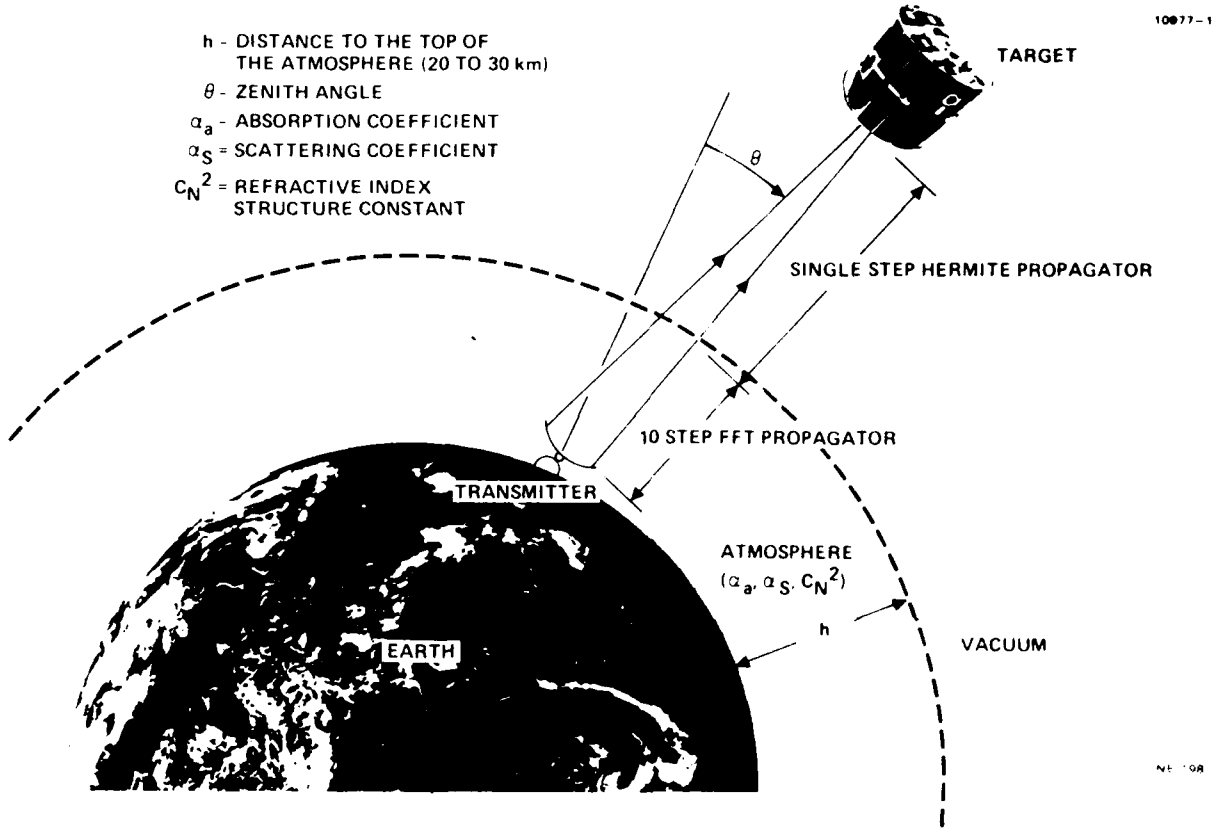

Figure 1. Atmospheric propagation model.

studies). This calculation employs a converging coordinate propagation code that utilizes a discrete Fourier transform technique to propagate from step to step. Although the steps taken with a converging coordinate code are generally not equally spaced, they were roughly equal in the simulations performed on this contract because the atmospheric propagation occurs in the near field of the transmitting aperture. The propagation from the top of the atmosphere to the relay satellite is performed with a single-step Hermite propagator. We use the Hermite propagator here instead of a FFT propagator because of the increased flexibility it affords us in the representation of the field at the relay mirror ... the Hermite approach allows us to "zoom in" on the field to represent a particular portion with greater detail than can be done conveniently with a FFT propagator.

The effects of atmospheric turbulence are accounted for by introducing a two-dimensional random phase screen at each propagation step (see Figure 2). These screens simulate the phase distributions produced by Kolmogorov turbulence. They are generated by evaluating a Fourier integral representation of a sample realization via a discrete Fourier transform approximation to this integral.[5] The screens are characterized by the outer scale length of the Kolmogorov spectrum and the mean square fluctuation in the phase (which is a function of the thickness of the

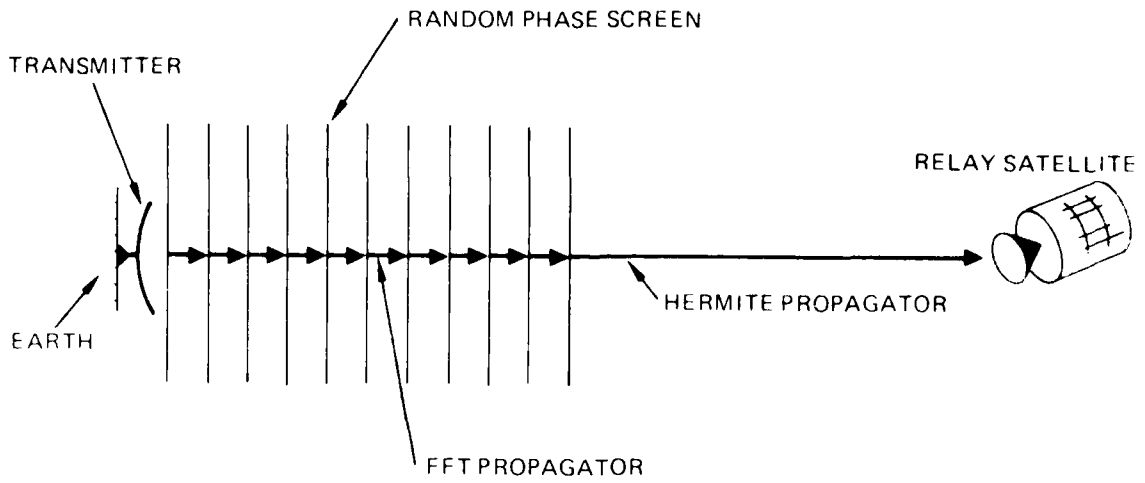

Figure 2. Turbulence modeling.

atmospheric layer that the screen represents and the magnitude of the refractive index structure constant within this layer). The inner scale length is determined effectively by the distance between mesh points. The accuracy of the modeling has been verified by checking the statistical properties of the generated screens against the known properties of phase fluctuations produced by Kolmogorov turbulence; e.g., the mean square value and structure function of the fluctuations. The variation in the strength of the turbulence with altitude is represented by the Miller-Zieske day and nighttime models[7] for the index structure constant. These models are based on data taken at the AMOS observatory located at Maui, Hawaii. Figure 3 shows these profiles. Although it was not used in the work performed on this contract, the code also has a structure constant model based on the profile suggested by Hufnagel.[8] In contrast to the Miller-Zieske models, this profile has a tropopause "bump" that tends to accentuate the effects of anisoplanatism.

The propagation code is time dependent in the sense that the properties of the atmosphere are allowed to vary in time. In general, this includes a time dependent solution of a set of hydrodynamic equations that describe the changes in air density caused by absorptive heating (which leads to

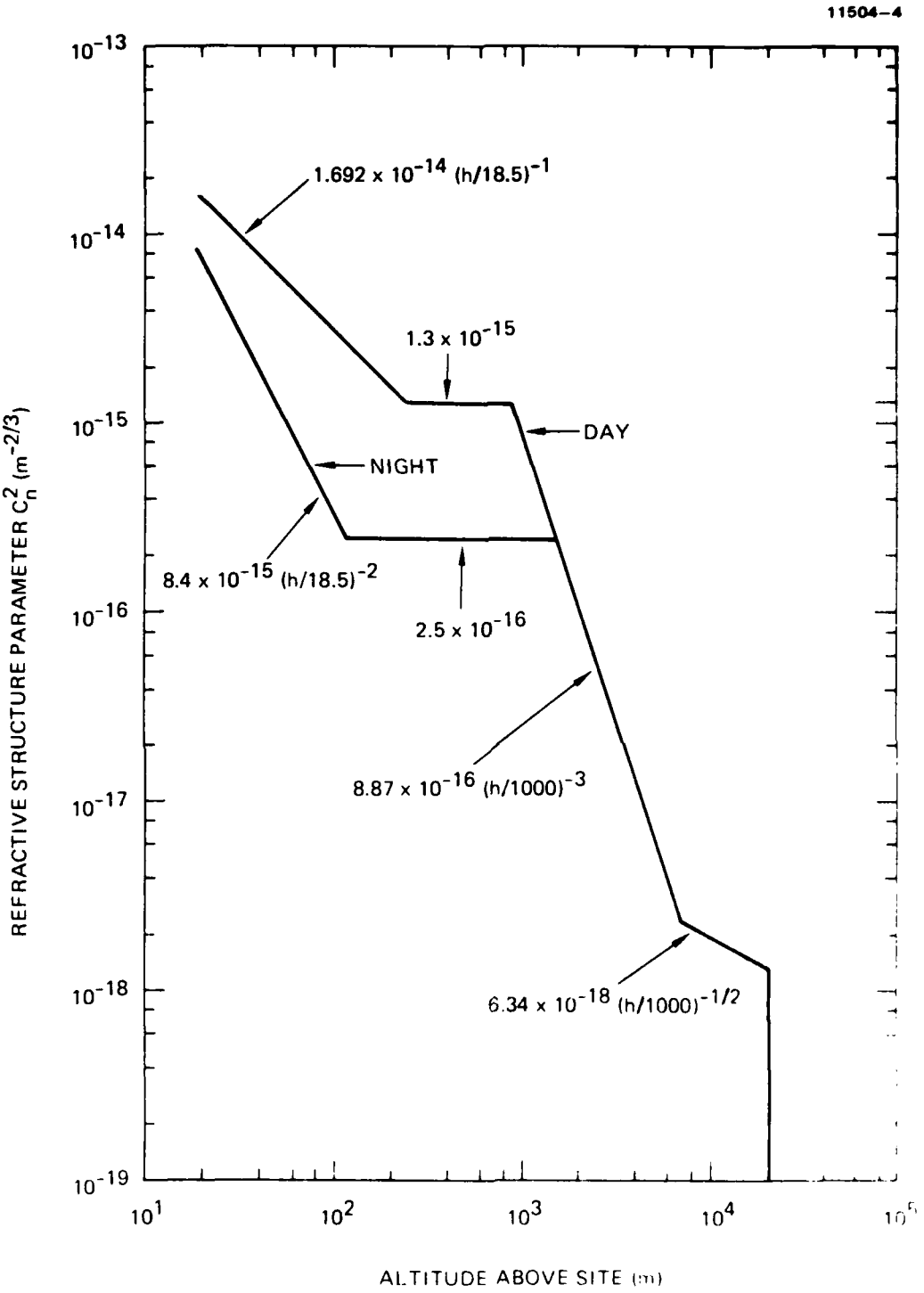

Figure 3. Miller-Zieske refractive index structure constant profiles.

thermal blooming effects) and a time dependent modeling of the contributions due to turbulent inhomogeneities. This allows us to account for the effects of the temporal variation in the propagated and reference fields used in the adaptive optics simulations. Since thermal blooming was only a secondary concern in these studies, we will not discuss the time dependent hydrodynamic modeling here (see reference 5). The temporal variation of the turbulence is modeled by shifting the random phase screens along the direction of the local wind velocity. This approach is based on the assumption that the turbulence satisfies Taylor's frozen turbulence hypothesis,[3] which states that the temporal variation in the turbulence observed at a point is due in large part to the transport of the turbulent eddies intact via the local wind. The distance that a random phase screen is translated depends on the product of the time increment and the local wind velocity at the altitude of the screen. We have used the wind velocity profile shown in Figure 4. This profile is based on data taken at Maui. In order to accommodate the translation of the screens, we generate these screens on a mesh that is twice as large as the propagation mesh along the direction of the wind and equal to the propagation mesh along the

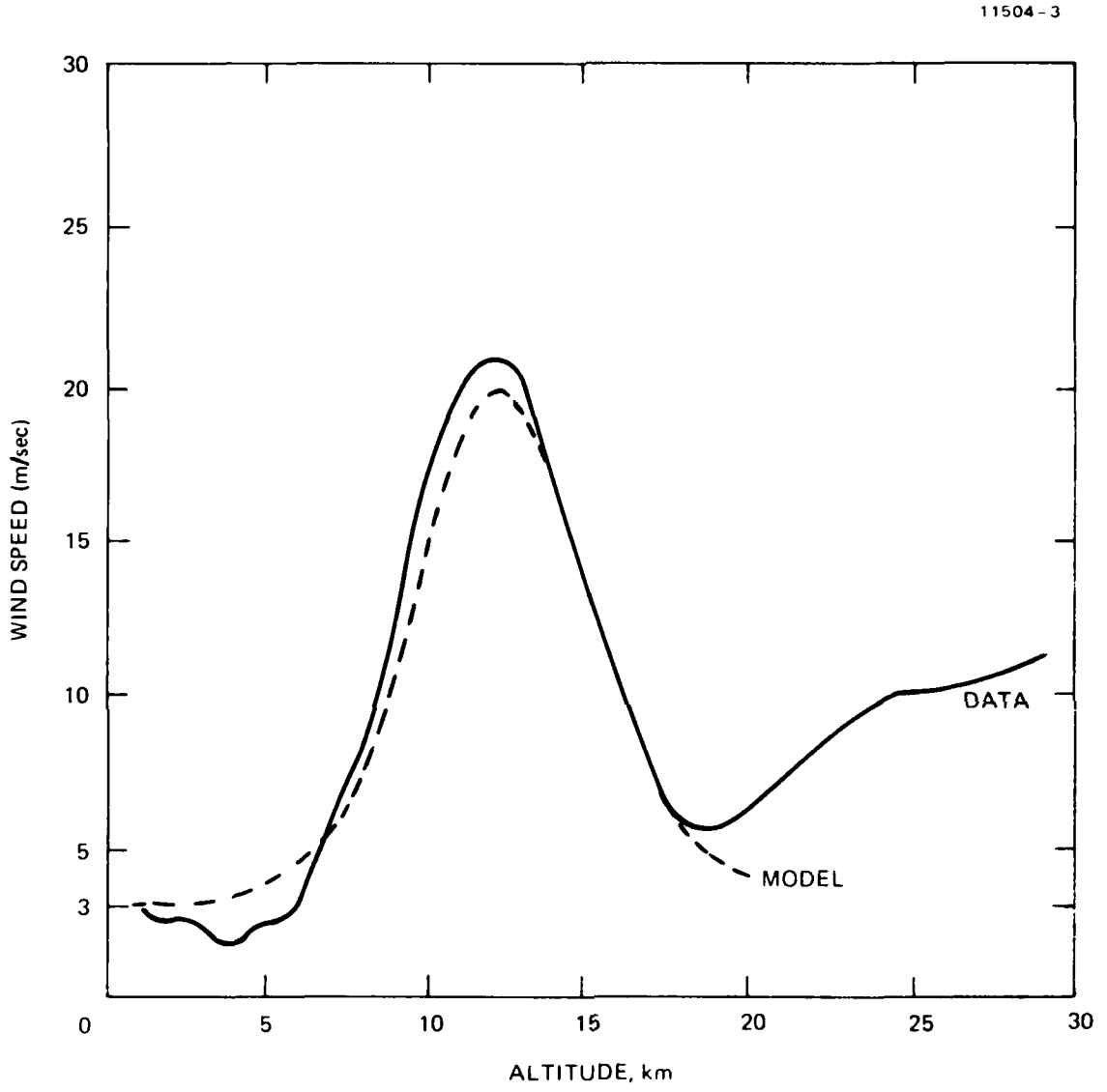

$$V_{WIND} = 3 + 17 \exp(-(h-12.5)^2/16)$$

Figure 4. Wind velocity model.

orthogonal direction; i.e., we use a 512 x 256 mesh for the screens when the propagation mesh is 256 x 256.

It is assumed in the simulation that the principal absorbers at .5 μm are ozone and aerosols, and the principal scatterers are aerosols and air molecules. The model used for ozone absorption is based on a fit to the data presented in the Handbook of Geophysics and Space Environments.[9] The aerosol absorption model is based on a fit to the data of Elterman.[10] The relations used in the code are

$$\ln(\text{alpha}_{\text{ozone abs}}) = \begin{cases} -8.2929 - .128\,h, & 0<h<4 \\ -8.8049, & 4<h<8 \\ -10.9404 + .267\,h, & 8<h<13 \\ -8.5411 - .0824\,h, & 13<h<23 \\ -3.8859 - .12\,h, & h>23, \end{cases} \quad (1)$$

$$\ln(\text{alpha}_{\text{aerosol abs}}) = \begin{cases} -4.442 - .768\,h, & 0<h<3 \\ 5.850 - .292\,h, & 3<h<6 \\ -7.544 - .0096\,h, & 6<h<17 \\ -4.172 - .208\,h, & h>17, \end{cases} \quad (2)$$

where h is the altitude above sea level in kilometers. The aerosol and molecular scattering models are based on a fit to the data presented in the Handbook of Optics.[11] The relations used in the code are

$$\ln(\text{alpha}_{\text{aerosol sc}}) = .17\exp(-.827h^{1.1}) + 4.53\times10^{-3} - .000107h, \quad (3)$$

$$\ln(\text{alpha}_{\text{molecular sc}}) = 2.02\times10^{-2}\exp(-.113h). \quad (4)$$

2.2 Adaptive Optics Modeling

The adaptive optics software used during this contract models a return-wave, phase-conjugate adaptive-optics system. It is assumed in the modeling that a reference wave is propagated from a beacon satellite that is located ahead of the relay satellite. As shown in Figure 5, the modeling accounts for beacons positioned at arbitrary angular offsets from the point-ahead direction, which allows us to model the effect of beacon station-keeping errors and also cases in which the beacon is located on the relay satellite. The reference wave is propagated back to the ground station receiver where the wavefront is sensed and the appropriate correction profile applied to the transmitted wave. In propagating the reference wave, we utilize the same turbulent medium used in the modeling of the propagation of the transmitted wave. The effect of the difference in the paths taken by the transmitted and return waves is modeled in the manner indicated in Figure 6. In order to reduce the

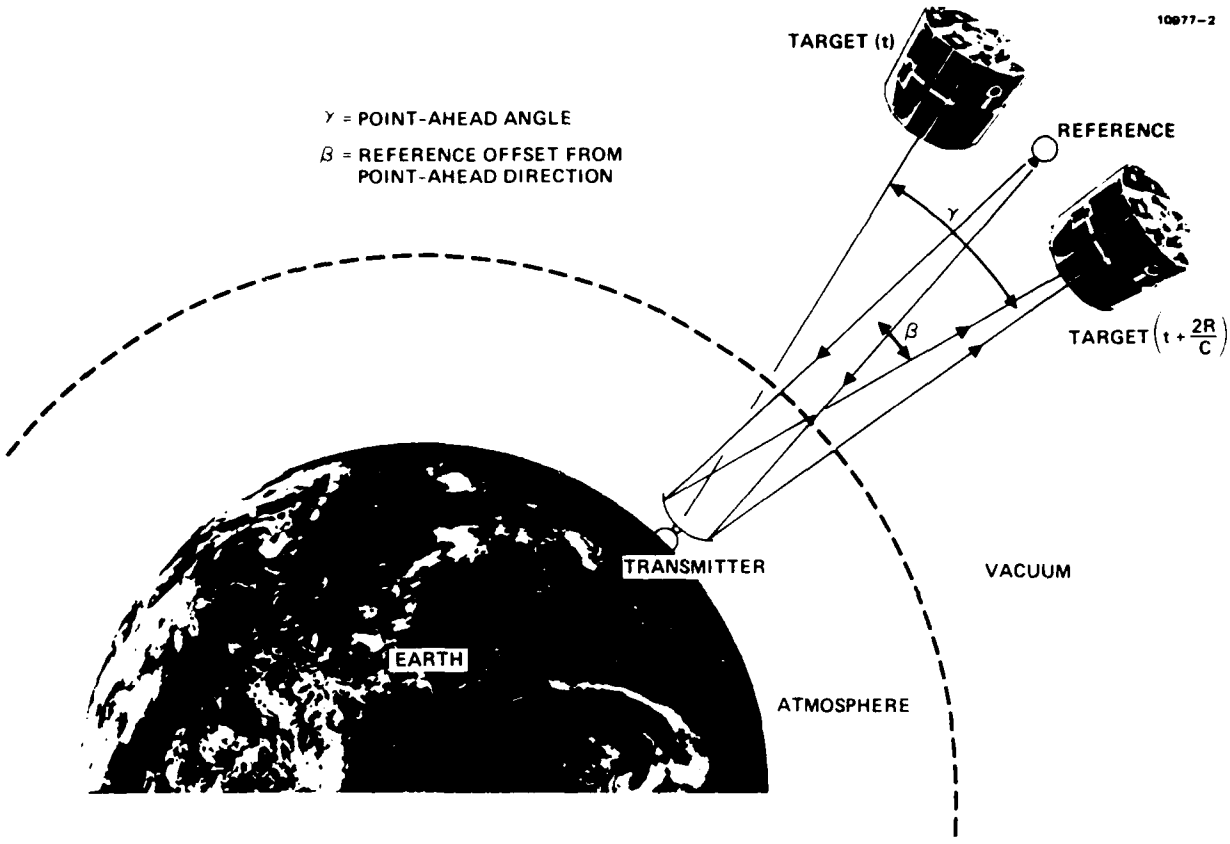

Figure 5. Target/reference geometry for adaptive optics modeling.

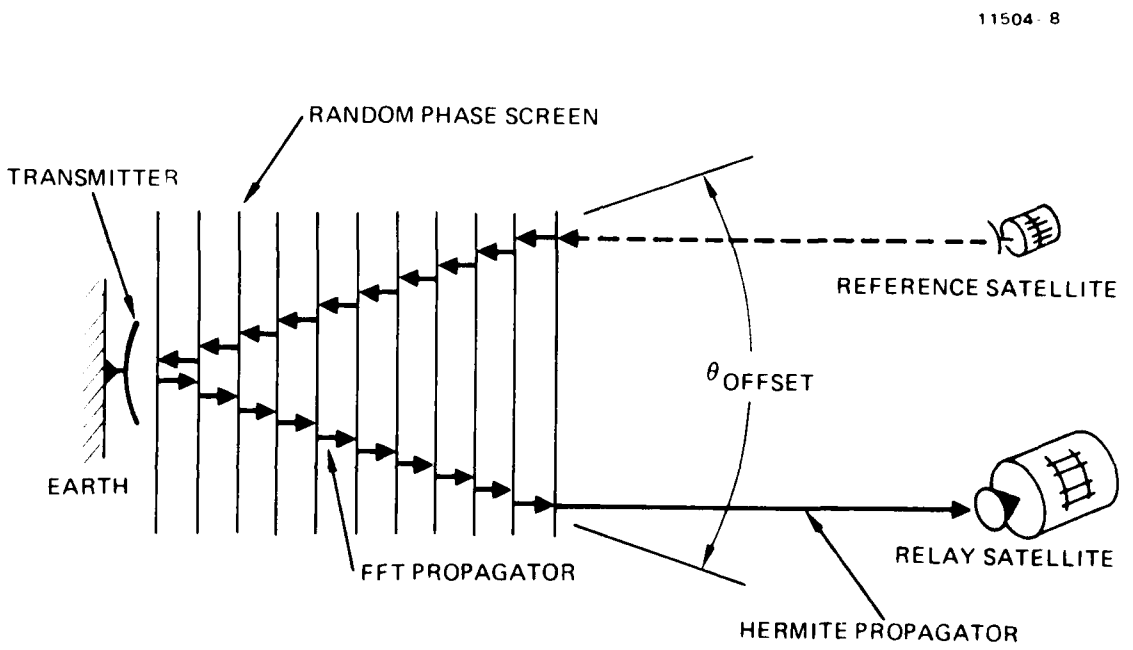

Figure 6. Offset reference modeling.

sampling requirements, we do not actually introduce the wavefront tilts corresponding to their different directions of propagation. Rather, as indicated in Figure 6, we account for the associated beam displacements by oppositely directed displacements of the waves at each propagation step.

The phase of the reference wave is sensed and the corresponding correction applied to the transmitted wave via the servo system model depicted in Figure 7. This model consists of a deformable corrector mirror, a phase-difference sensor, an optimal estimator used to convert phase differences to actuator settings, and a low-pass filter used to represent the finite temporal response of the adaptive-optics system. The reference wave is reflected from the deformable mirror yielding a wave having a phase that is equal to the difference between the mirror profile and the phase of the reference wave. This phase distribution is the "error signal" that the servo tends to drive to zero. Note that if the deformable mirror had a profile that exactly duplicated the negative of the reference wave phase, the error signal would be zero. Thus, the servo tends to set the deformable mirror to a profile corresponding to the phase of a wave that is the complex conjugate of the reference wave.

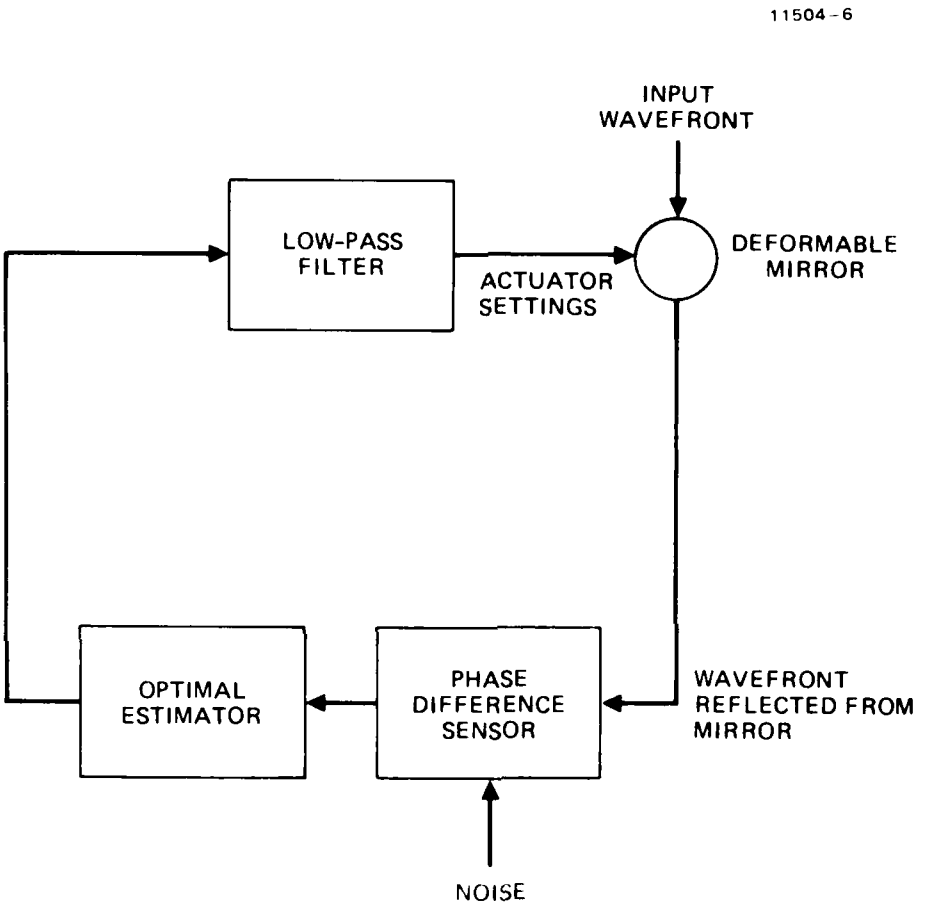

Figure 7. Servo system modeling.

The phase-difference sensor used in the simulations performed on this contract approximates the performance of a shearing interferometer wavefront sensor. The elements of this model are shown in Figure 8. The wavefront of the wave reflected from the deformable mirror enters a phase-difference sensor that measures a set of x and y phase differences defined on a set of sub-apertures. A shearing interferometer performs these measurements by synchronously detecting the dynamic interference of the wavefront with a spatially-shifted, frequency-shifted replica obtained, for example, from a rotating Ronchi grating. To simplify the modeling, we approximate this process by a direct calculation of the sub-aperture phase differences from the input field data. As indicated in Figure 8, we then modify these phase differences to account for the way in which they are measured by a shearing interferometer. First, we reduce the magnitude of the differences by a factor s/d, which is the ratio of the shear distance to the linear extent of the sub-aperture. This accounts for the fact that the shearing interferometer does not measure the total phase-difference across a sub-aperture but instead a difference corresponding to the shear distance. Next, we take the sine and cosine of

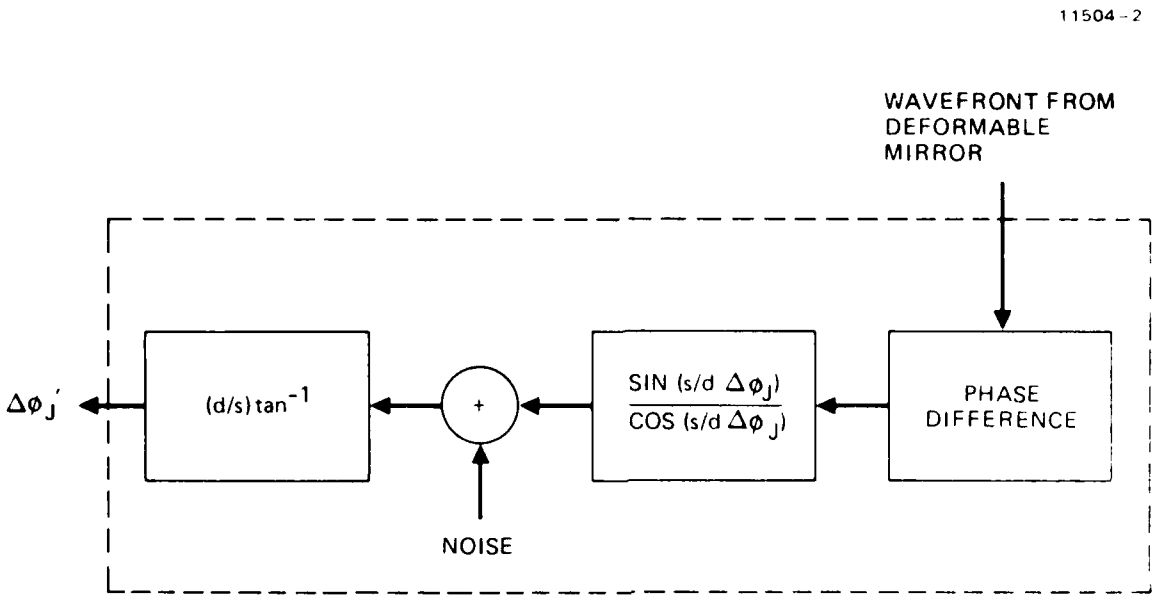

$$\Delta\phi_J' = (d/s)\tan^{-1}\left(\frac{\text{SIN}\,(s/d\,\Delta\phi_J) + N_s}{\text{COS}\,(s/d\,\Delta\phi_J) + N_c}\right)$$

Figure 8. Wavefront sensor modeling.

the differences, add independent components of noise, N_s and N_c, form the ratio, take an inverse tangent, and multiply by the inverse of the factor s/d. This is an approximate modeling of the phase detection process used in a shearing interfermeter sensor, which is based on the detection of zero-crossings of the synchronously detected signal associated with the wavefront interference.

The optimal estimator used in these studies is based on the work of Hudgin.[12] In our previous simlulations we had used another estimator based on an exact solution to the estimation problem. This approach had to be abandoned in these studies, however, since we found that the exact solution of the estimation problem requires too much computer time and memory when the number of actuators is large (as it is in the SLC Uplink problem). Thus, we modified the code to implement Hudgin's estimator, which is based on an approximate solution of the estimation problem and thereby requires significantly less computer memory and time to solve. In this approximation, which neglects mirror edge effects and therefore is most accurate for large actuator arrays, the best set of actuator positions ϕ_j (j=1,N; N=number of actuators) is related to the phase differences $d\phi_q$ (q=1,M; M=number of phase difference measurements) by the following Poisson difference equation

$$\phi_j = .25(\phi_m + \phi_n + \phi_p + \phi_q$$

$$+ d\phi_u - d\phi_s + d\phi_t - d\phi_r), \quad (5)$$

where the actuators m,n,p and q are the four nearest neighbors of the j^{th} actuator and the differences dO are directed as indicated in Figure 9. The above relation applies to interior actuators. In the case of edge actuators and corner actuators the same type of relation applies except that the missing neighboring actuators and differences are deleted and the coefficient in front is changed to 1/3 for edge actuators and 1/2 for corner actuators. We solve these relations by iteration starting from an initial guess (which is obtained from the solution obtained for the previous servo time increment).

The low-pass filter models a simple RC type of response. This yields a type zero servo. A second-order Runge-Kutta algorithm is used to solve the filter equations. The servo bandwidth (BW) and time increment are input parameters to the code. To ensure that an adequate number of time samples are processed, we typically set the time increment equal to .1/BW.

Finally, the servo loop is closed by applying the low-pass filtered actuator settings to the deformable mirror. It is assumed that the mirror responds instantaneously to these settings, the finite response time

of the mirror having been included in the low-pass filtering. The mirror is characterized in the modeling by the number of actuators and an unconstrained influence function P(r) calculated from thin plate theory[13]

$$P(r) = 1 - (r/a)^2 + .8(r/a)^2 \ln(r/a) \quad . \quad (6)$$

This relation gives the displacement of a thin, flat, circular plate of radius "a" pushed upward at its center by a zero width actuator. The plate is unconstrained except at the outer edge where the displacement is set to zero. It is assumed that the mirror radius is small compared to the radius a that appears in the above relation. The mirror profile is determined from the actuator positions b_n (n=1,N) and the influence function P in two steps. First, we determine a set of forces f_n that produce the known mirror displacements at the actuator locations. This is done by solving the following set of linear equations

$$b_m = \sum f_n \, P(x_m - x_n) \quad , \quad (7)$$

where x_m and x_n denote the location of mirror actuators. The mirror profile is then calculated via the relation

$$\phi(x) = \sum f_n \, P(x - x_n) \quad , \quad (8)$$

where x now denotes the location of a general point on the mirror surface.

III. COMPUTER CODE MODIFICATIONS

Although the fruits of the code modification task are not readily obvious to those not involved in the details of the simulations, this work consumed a substantial fraction of the total contract effort. In addition to those modifications that had been planned on to upgrade the HRL simulation such as an increase in the size of the propagation mesh and a modification of the technique for generating the random phase screens used to represent the effects of atmospheric turbulence, we had to make additional substantial changes in the software to accommodate operation on the new AFWL Cray-1 computer. In terms of time spent, the conversion effort was easily the most demanding. The additional work was compensated, however, by the greatly increased performance capabilities of the code once it was converted to the Cray. The increased storage capacity and speed of the new machine were particularly important to the eventual success of the simulation studies. The available memory on the AFWL Cray is almost double that available on the CDC 7600 machine that we originally planned to use. In addition, the vector processing capabilities of the Cray, coupled with a favorable rate schedule, enabled us to reduce the cost per run by about a factor of two over what it would have been on the CDC 7600. The code modifications performed

on this contract are summarized in the following paragraphs.

3.1 Compatibility With The Cray-1

The principal difference between the Cray-1 and the CDC 7600 is the fact that the Cray has a vector processing capability. By this we mean that the machine architecture is such that it can perform different floating point operations such as add, multiply and fetch simultaneously and can process any of these operations on vector arrays effectively at the rate of one per clock cycle. In order to take advantage of this capability, however, there are a limited set of rules that must be satisfied. Considerations include: (1) vectorization occurs only within the innermost do loops; (2) certain operations inhibit vectorization ... these include, conventional Fortran conditional branching statements, subroutine or function calls, most forms of integer arithmetic, indirect addressing, and recursiveness; and (3) maximum speed requires care in the way in which array elements are stored and retrieved from memory. Actually, the Cray Fortran compiler has a switch that allows the user to turn off the vectorization, in which case it is almost completely compatible with the CDC 7600 compiler. But, even if we had adopted this approach, we would have had to modify portions of the code since some of the library routines such as the FFT were written in CDC assembly language. Another disadvantage of this approach is that, in spite of the fact that the Cray has a clock rate twice that

of the CDC 7600, the speed of serial arithmetic performed on the Cray tends to be equal to or somewhat less than that of the 7600. This is caused by the relatively unsophisticated nature of the Cray compiler compared to the highly optimized version available on the 7600.

The simulation software was modified to be consistent with the requirements for vectorization wherever possible. This entailed a considerable number of changes that involved rewriting multiple do loops in such a way that the modified version was compatible with vectorization. The routines used in the mirror modeling, the servo-loop modeling, the turbulence modeling, and the Hermite propagation required substantial modification to achieve this goal. In addition, it was necessary to modify the manner in which data are stored in memory since the Cray has only one central memory unit rather than being divided into small and large core memories as is done on the CDC machines. We also had to write some new software such as the two-dimensional FFT mentioned above.

3.2 Other Code Modifications

The size of the propagation mesh was increased from a 64 x 64 mesh up to a maximum size of 256 x 256. This increase was made possible partly by the increased size of the Cray memory and partly by a change in the way that the random phase screens are stored. We now store the screens

on disk rather than in the random access memory and thereby have increased the amount of memory available for the remainder of the program. This change also gives us the capability of using larger random phase screens in problems where it is necessary to simulate long servo runs. It is a much cleaner and versatile solution to this problem than the techniques considered at the outset of this contract; e.g. utilizing a single large screen on which the propagation mesh is circulated.

In addition to increasing the maximum size of the propagation mesh, we have made it substantially easier to change from one mesh size to another. This was accomplished by using parameter statements to define the various array dimensions. Changing the dimension of the propagation mesh and all related array dimensions now requires only the modification of one program statement, whereas the previous version of the code required that many lines of code be changed to do the same thing. Likewise, we have made it much easier to change the number of mirror actuators by using the same technique.

The wavefront sensor and mirror modeling software was upgraded to allow the simulation of systems having significantly more actuators than was previously possible. In the process of making these changes we realized that the optimal estimation procedure originally implemented to

determine the actuator positions from the phase-difference data cannot be used for systems having the extremely large numbers of actuators required in the SLC Uplink system (up to 1000 or more). The problem is associated with the fact that this estimation procedure requires the calculation and storage of an estimator array have the dimension N_{meas} x N_{meas} where N_{meas} is the total number of phase-difference measurements. Since the number of measurements is approximately twice the number of actuators, the estimator array for a 1000 actuator system requires approximately $4x10^6$ words of memory, which is well beyond the storage capability of the computer. The basic problem with this approach is that it is an exact procedure which does not take advantage of the inherent sparseness of the estimator array. The approximate estimation technique developed by Itek for the lateral shearing interferometer sensor[12] requires substantially less memory. Thus, we modified the software to include their estimation algorithm (see Section II).

The need for another modification became apparent during the course of the simulation of the effects of anisoplanatism. The results obtained originally for these effects taken separately with no other errors present did not agree with those obtained from the theoretical predictions. The Strehl ratio at large angular offsets from the point-ahead direction were higher by about 30 to 40

percent than the theoretical predictions. We realized that this discrepancy might be caused by the discrete representation of the atmosphere used in the simulation. The effect of atmospheric turbulence is represented by 11 discrete phase screens, the first of which is located directly in front of the transmitter. This screen represents the effect of the turbulence located in the first kilometer above the transmitter. The contribution of the this turbulence to the anisoplanatic effect was not taken into account in the early simulations since it was located directly in front of the transmitter and the reference and transmitted waves thus transited this screen at the same point. Thus, we modified the code to account for the difference in the phase variations contributed by this turbulence to the reference and transmitted waves. This was accomplished by shifting the first phase screen a small distance in the direction of the reference in the case of the reference wave propagation and in the opposite direction in propagating the transmitted wave; thereby, approximately accounting for the difference in the paths taken by the reference and transmitted waves (see Figure 6). The results obtained with the modified code agree quite well with the theory.

IV. SIMULATION RESULTS

A number of simulations were performed to delineate the effects of atmospheric turbulence on the SLC Uplink system and the ability of a phase-conjugate, adaptive-optics system to compensate for these effects. The manner in which these simulations were performed and the nature of the results obtained are discussed in this section.

4.1 Conditions, Procedures, and Sample Results

In order to limit the parameter space we selected a canonical set of system and atmospheric parameters to use in the simulations. The canonical system utilizes .5 μm radiation and an unobscured 1 meter transmit-receive aperture. The adaptive-optics system has a deformable mirror having from 38 to 346 actuators. We also simulated systems having a "perfect" mirror which effectively had an actuator at every mesh point. This type of mirror was used in those simulations in which the spatial frequency response of the mirror is theoretically infinite. We chose to limit the transmit-receive aperture to 1 meter to ensure that the spatial sampling of the medium and the fields was adequate. The effect of spatial sampling was explored by comparing results obtained with 128 x 128 and 256 x 256 propagation meshes. Generally, the results obtained with the two meshes

agreed quite well, which indicates that the sampling was adequate. We found that the simulations involving the effects of anisoplanatism were the most sensitive to changes in the mesh, and therefore used the finer 256 x 256 mesh for the bulk of these simulations. The fact that we simulated a system having a smaller transmit-receive aperture than that contemplated in the SLC Uplink application is of no great consequence since the results are not strongly dependent on aperture size (assuming, of course, that the number of mirror actuators per unit area of the transmit-receive aperture is fixed).

Simulations were performed with both the day and nighttime Miller-Zieske structure constant profiles. The daytime profile was used for propagation along two different paths: (1) a zenith path; and (2) a path slanted 45^{o} to the zenith. The nighttime profile was used only for propagation along the zenith. The phase coherence length associated with the daytime profile is 5 cm. for the zenith path and 4 cm for the path slanted at 45^{o}. The phase coherence length for the nighttime profile is 10 cm.

The atmospheric propagation of a wave from a ground-based transmitter to a relay satellite is a stochastic process and therefore is best described in terms of its statistics. Although a complete description of the statistics of this problem cannot be obtained from the

limited amount of data that can be economically obtained via a detailed computer simulation of the type performed on this contract, it is practical to obtain information pertaining to the average value of the irradiance received at the relay mirror and an indication of the degree to which the irradiance fluctuates about this mean. To obtain these data, we performed a set of 6 runs for each case of interest. In each of these runs a unique set of random phase screens was generated to create a sample random medium. A Strehl ratio defined as ratio of the peak irradiance at the relay mirror to the theoretical maximum irradiance obtainable in the absence of inhomogeneities was calculated for each run. We processed the results obtained from the 6 runs to obtain an average Strehl ratio and a normalized fluctuation about this mean. The fluctuation was defined as the ratio of the standard deviation of the results divided by the mean; i.e., the percent variation about the mean. Unless otherwise noted, the Strehl ratio and fluctuation results discussed later in this section were obtained in this manner. The fluctuation results are indicative not only of the degree of variation in the irradiance at the relay mirror but also of the accuracy of the results obtained for the mean Strehl ratio. The error incurred in calculating the mean value of a random process from a set of N statistically independent samples is equal to the standard deviation of the process divided by

$N^{1/2}$.[14] Thus, the fluctuation, as defined above, divided by $6^{1/2}$ (=2.45) is a measure of the accuracy of the associated mean Strehl ratio.

In order to give a perspective of the type of results that are obtained for the SLC Uplink scenario, we show in Figures 10-13 results obtained for a single atmospheric realization rather than the average results discussed above. These results apply to daytime propagation along a zenith path. Figure 10 shows the irradiance distribution in the vicinity of the relay mirror with the adaptive-optics system turned off. The shaded oval region is on the boresight axis and has an extent equal to that the Airy disk of a diffraction-limited system. An overprinting routine having ten greyscale levels was used to produce this plot (and those that follow). The magnitude of the irradiance is related to the darkness of the plot, with the darkest regions being most intense. All irradiance values less than 10% of the peak value are represented by a blank (i.e., no printed symbol at all). It is apparent from this result that the irradiance at the relay mirror will not only be considerably reduced below the diffraction limit, but will also fluctuate significantly since the irradiance distribution will tend to move about and change with time.

OBJECTIVE:

DETERMINE THE 'BEST' SET OF ACTUATOR POSITIONS FROM A NOISY SET OF WAVEFRONT SLOPE MEASUREMENTS

SOLUTION (ITEK):

$$\phi_J = 0.25\,(\phi_M + \phi_N + \phi_P + \phi_Q + d\phi_U - d\phi_S + d\phi_T - d\phi_R)$$

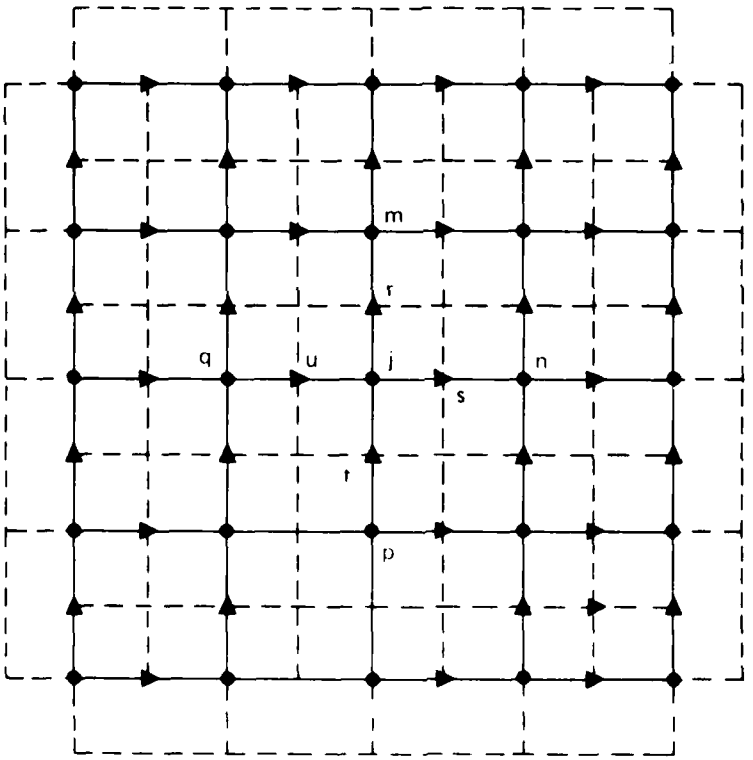

Figure 9. Actuator setting via optimal estimation.

Figure 11 shows the irradiance distribution obtained for the same atmospheric realization with an adaptive-optics system having a 133 actuator deformable mirror, infinite temporal bandwidth and signal-to-noise ratio, and a reference beacon situated such that the anisoplanatic effects are eliminated (reference located at the point-ahead angle). This irradiance distribution is centered on the boresight axis. Although the irradiance distribution appears to be almost diffraction-limited, it has a Strehl ratio of approximately .5 . This result is typical of the type of irradiance distribution obtained with moderate to high performance adaptive-optics systems. There is a well-formed central peak having a width comparable to that of a diffraction-limited beam, surrounded by a sidelobe structure that extends well beyond the limits of the Airy disk. The sidelobe structure is not apparent in Figure 11 because the irradiance values associated with this structure are less than 10% of the peak and therefore do not appear on the greyscale plot.

Figure 12 shows the phase profile introduced by the deformable mirror in the above system. The total phase excursion in this profile is 37 radians. This implies that the mirror must have an excursion capability exceeding plus or minus 3 waves (actually, the excursion requirements are

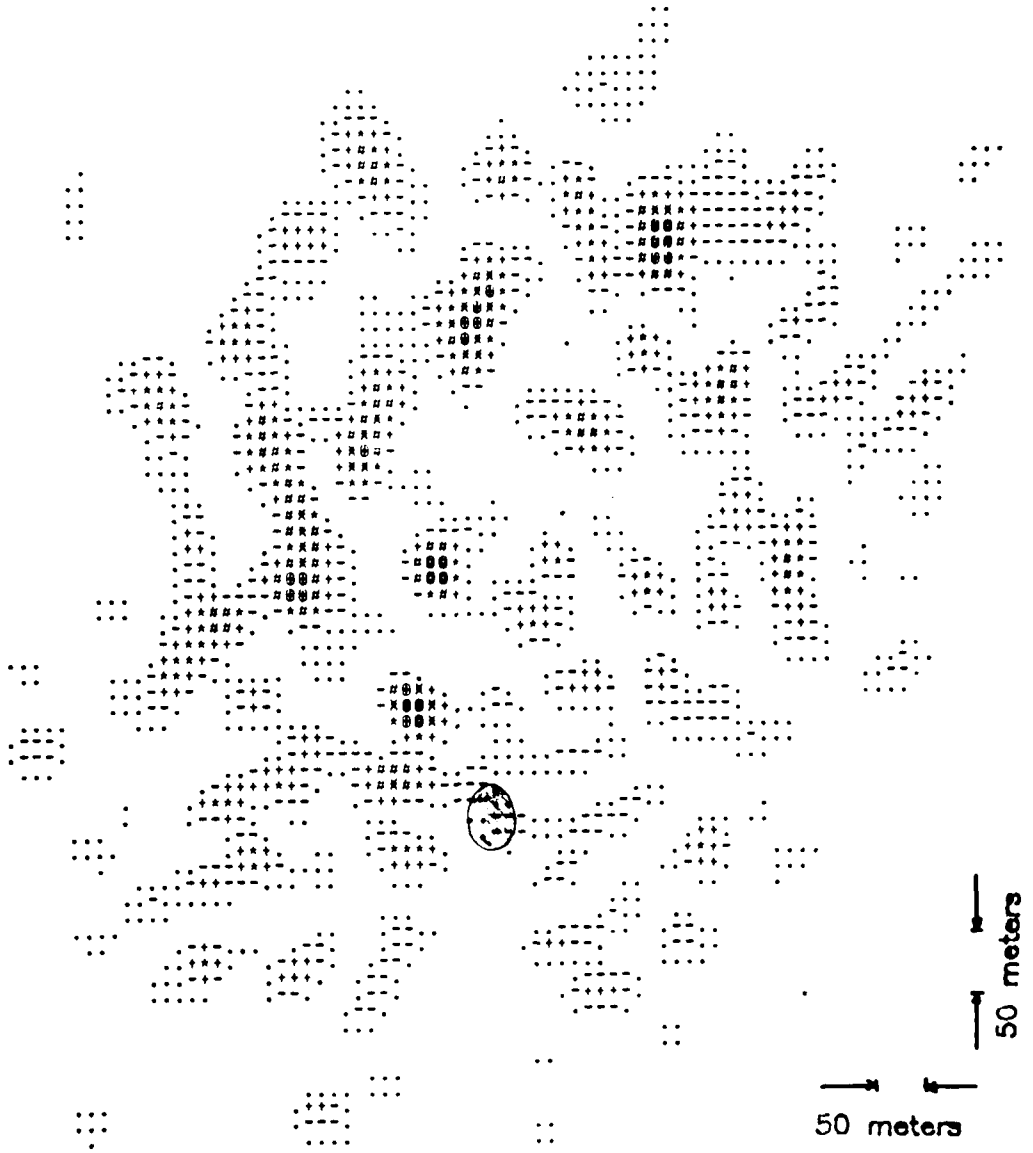

Figure 10a. Sample realization of an uncorrected irradiance distribution at the relay mirror. The shaded oval region denotes the size of the Airy disk of a diffraction-limited 1 meter transmitter; approximately 50 meter in extent, as indicated.

GREY-SCALE CHARACTERS

Figure 10b. 10-level greyscale used in the overprinting routine. The largest magnitudes are represented by the darkest character and the smallest level by a blank character.

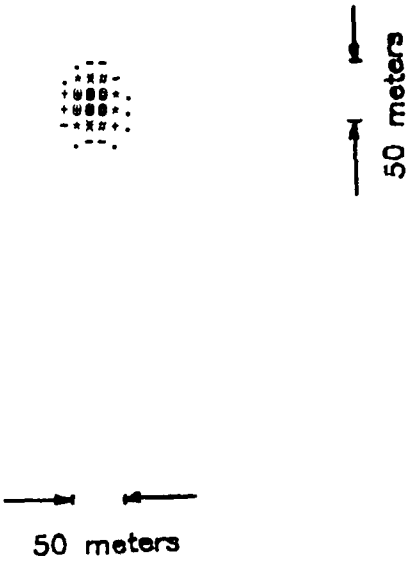

Figure 11. Sample realization of a corrected irradiance distribution at the relay mirror.

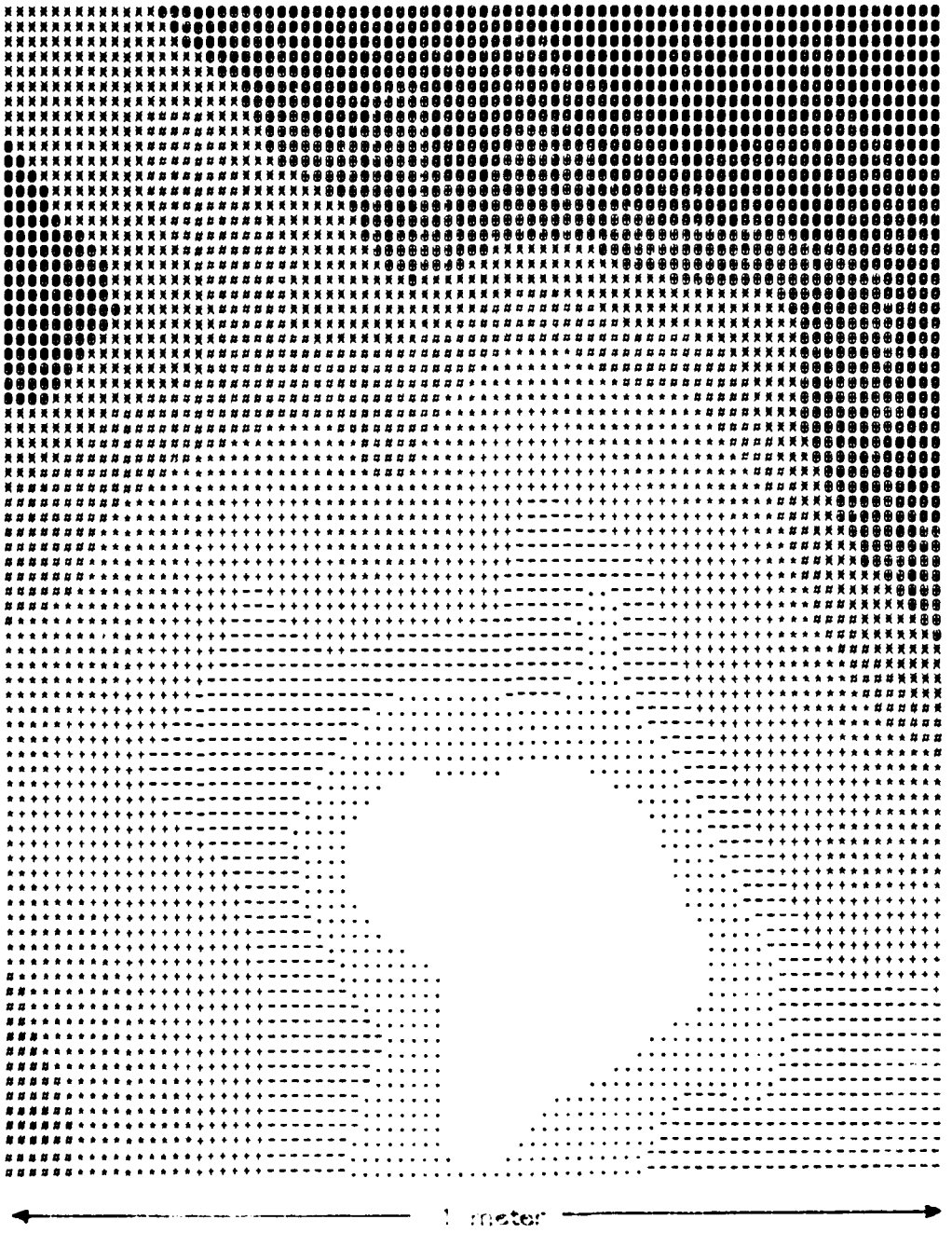

Figure 12. Sample realization of a deformable mirror profile. The total phase excursion in this sample is 37 radians.

less severe since it is likely that the adaptive-optics system will have a separate tilt mirror). Note that this plot is not representative of the mirror spatial frequency requirements since each grey level represents 3.7 radians of phase shift and therefore the mirror must be capable of introducing structure much smaller than that shown.

Figure 13 shows the irradiance distribution of the beacon at the receiver aperture in the above case. The irradiance is scintillating approximately 40% about the mean in this realization. This scintillation must be taken into account in the determination of the beacon power requirements.

4.2 Effect of Independent Errors

These simulations were performed to provide a comparison of the computer generated results with those obtained from the theoretical relations commonly used to predict the performance of adaptive-optics systems. The theoretical predictions are based on the assumption that the effects of errors caused by finite spatial bandwidth, finite temporal bandwidth, noise, and anisoplanatism are independent. Thus, we performed a set of simulations in which only one of the errors was present; e.g., a finite spatial bandwidth system having infinite temporal bandwidth, infinite signal-to-noise ratio, and no anisoplanatic error.

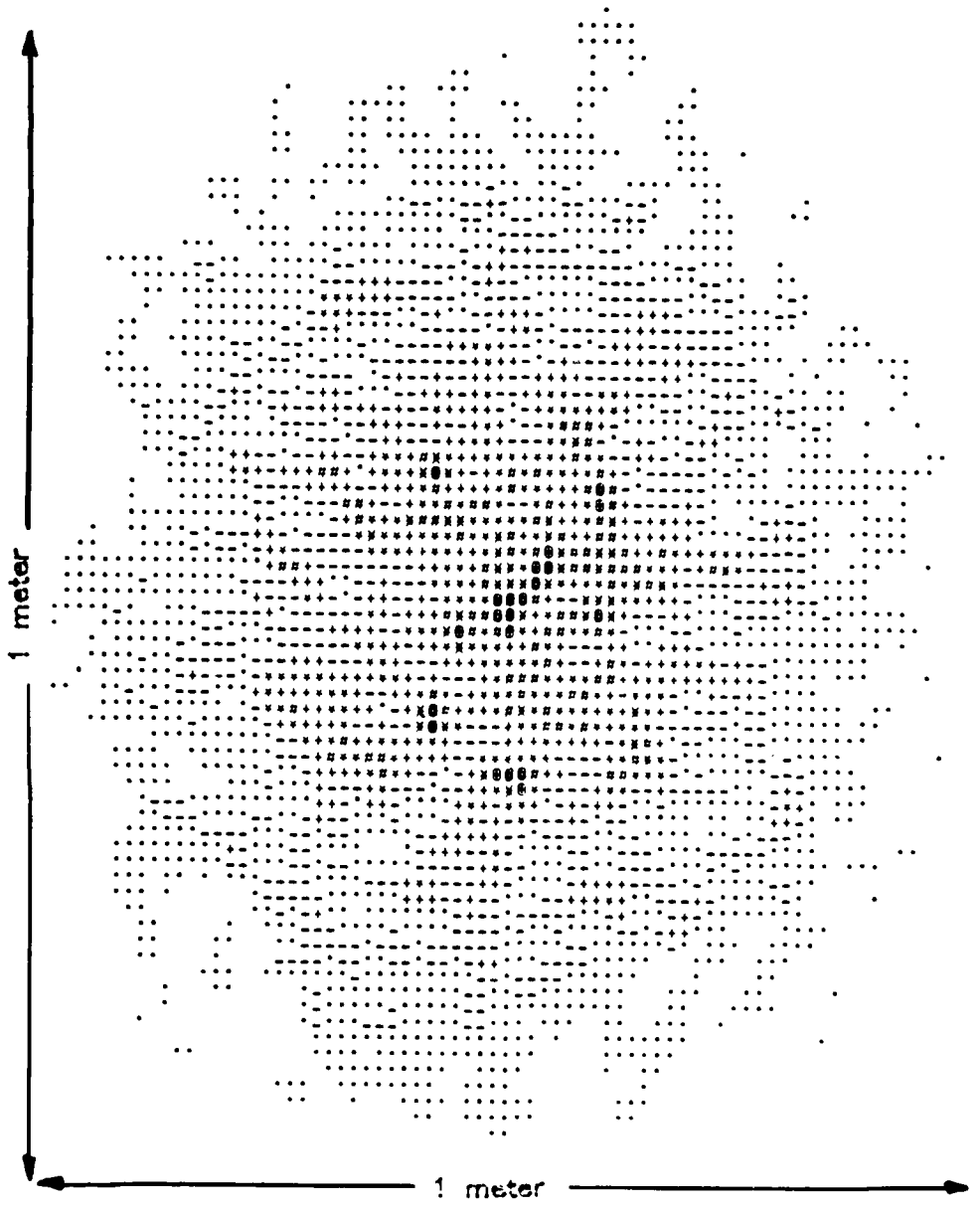

Figure 13. Sample realization of the irradiance distribution of the beacon at the receiver.

As discussed in the following paragraphs, we found that the results of such simulations agree quite well with the theoretical predictions. In addition to providing a measure of confidence that the computer software is free of bugs, this exercise yields information pertaining to the physics of the related propagation problem. The theoretical relations can be derived on the basis of a geometrical optics calculation of the propagation. Thus, agreement between the code results and the theory implies that the effects of diffraction are negligible; and consequently, that the analysis of the combined effects of the errors could also be based on a geometrical optics approach to the problem.[1]

4.2.1 Finite Spatial Bandwidth Effects

In these simulations we used a deformable mirror having a finite number of actuators. The reference and transmitted waves were propagated over the same atmospheric path (zero angular offset) thereby eliminating the effects of anisoplanatism. Although the servo model was used to set the actuator positions, the temporal bandwidth was effectively infinite because we held the medium and reference wave fixed at the values established at the first time increment (in contrast to the usual policy in which the

medium and reference wave change at each time increment). The servo signal-to-noise ratio was infinite.

Figure 14 shows the average Strehl ratio at the relay mirror as a function of the inter-actuator spacing normalized to the phase coherence length r_o. These results were obtained from simulations performed with three different atmospheric turbulence conditions: (1) Miller-Zieske daytime turbulence having an r_o of 5 cm.(propagation along the zenith); (2) Miller-Zieske daytime turbulence having an r_o of 4 cm. (propagation along a slant path at 45^o to the zenith); and (3) Miller-Zieske nighttime turbulence having an r_o of 10 cm. (propagation along the zenith). The theory curve is based on a relation supplied to us by RADC. We have previously derived a similar relation by calculating the mean square error incurred in fitting a finite-actuator deformable mirror profile to an atmospheric phase distortion. [5]

The agreement between the computer results and the theoretical relation is generally quite good except for some disagreement at very small and very large inter-actuator spacings. The disagreement near zero inter-actuator spacing is probably due to the effect of scintillation, which is neglected in the theory. The disagreement at large spacings is perhaps due to a difference in the influence function of simulated and theoretical mirrors.

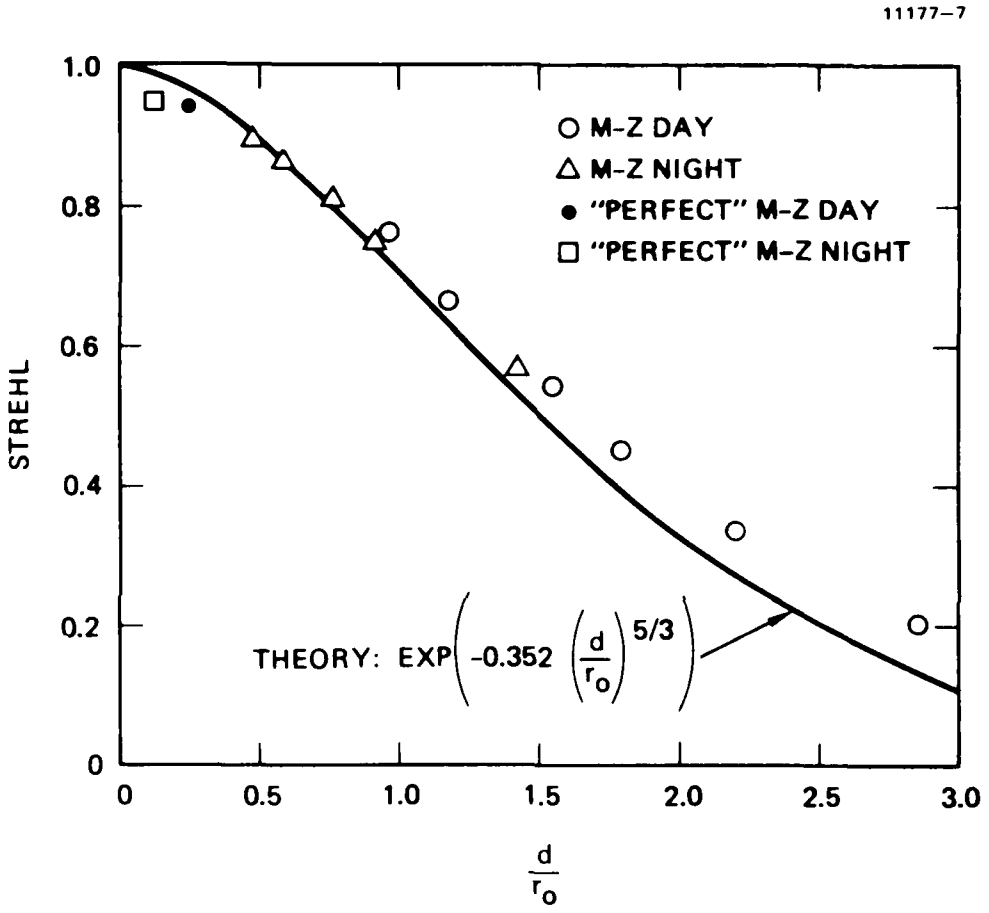

Figure 14. Average Strehl ratio versus actuator spacing.

4.2.2 Effects of Anisoplanatism

In these simulations the adaptive-optics system had infinite spatial bandwidth, temporal bandwidth, and signal-to-noise ratio. The effects of anisoplanatism were studied as a function of the angular offset of the reference beacon from the point-ahead direction (which is approximately 20 μrad. in front of the relay mirror if the relay satellite is in a synchronous orbit). The results of these simulations generally agree quite well with the predictions obtained from the theory developed by Fried,[16] who utilized an approach based on the Rytov solution of the propagation equations (the same results can be obtained from geometrical optics[17]). As mentioned in Section 4.1, we found that it was necessary to use a 256 x 256 propagation mesh in these simulations to obtain good agreement with the theoretical predictions. This implies that small scale phase fluctuations play an important role in the anisoplanatic effect.

Figures 15, 16, and 17 show the results obtained in these simulations. The results in Figure 15 apply to nighttime propagation along the zenith; those in Figure 16 to daytime propagation along the zenith; and those in Figure 17 to daytime propagation along a slant path at 45^{o} to the zenith. The discrepancy between the theoretical and

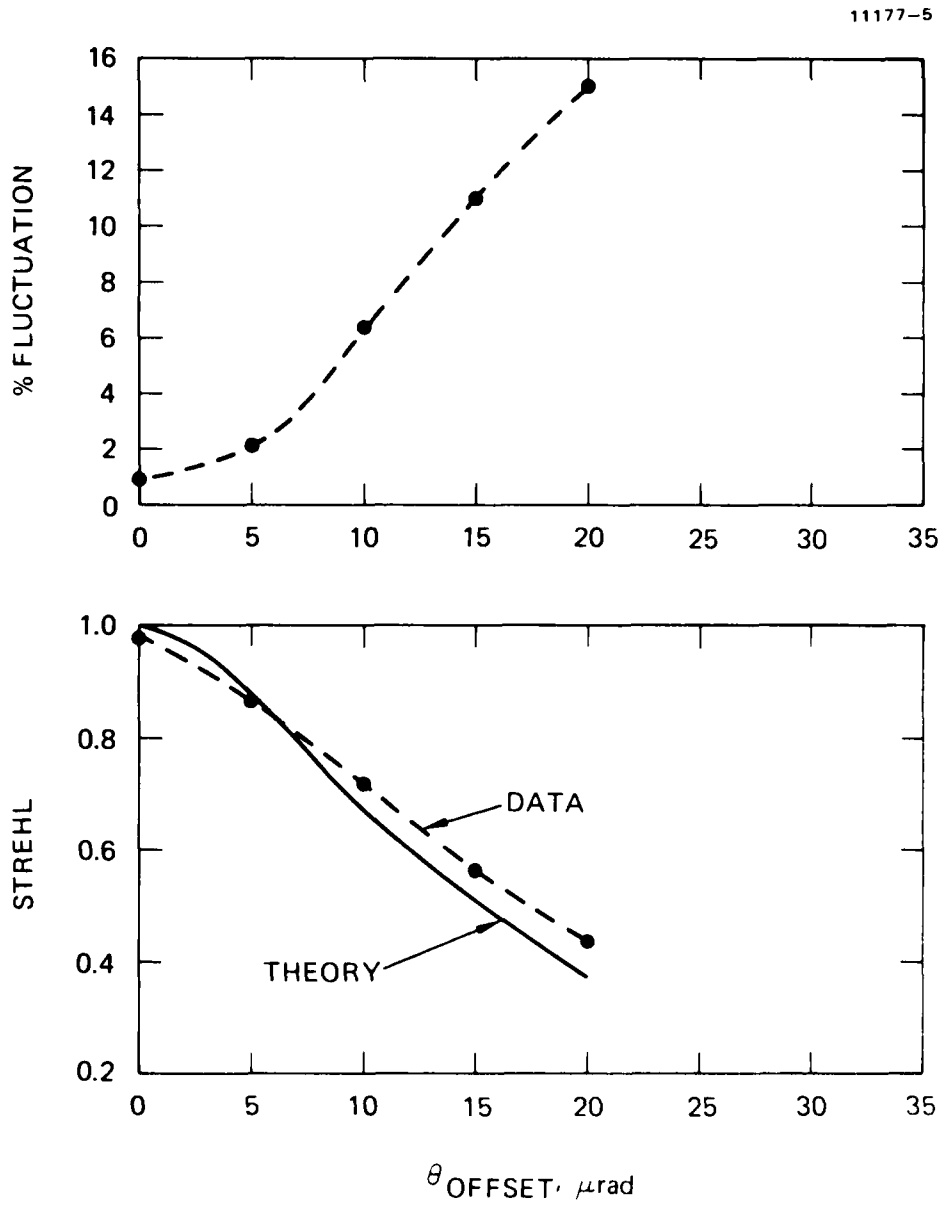

Figure 15. Anisoplanatism for nighttime propagation along a zenith path.

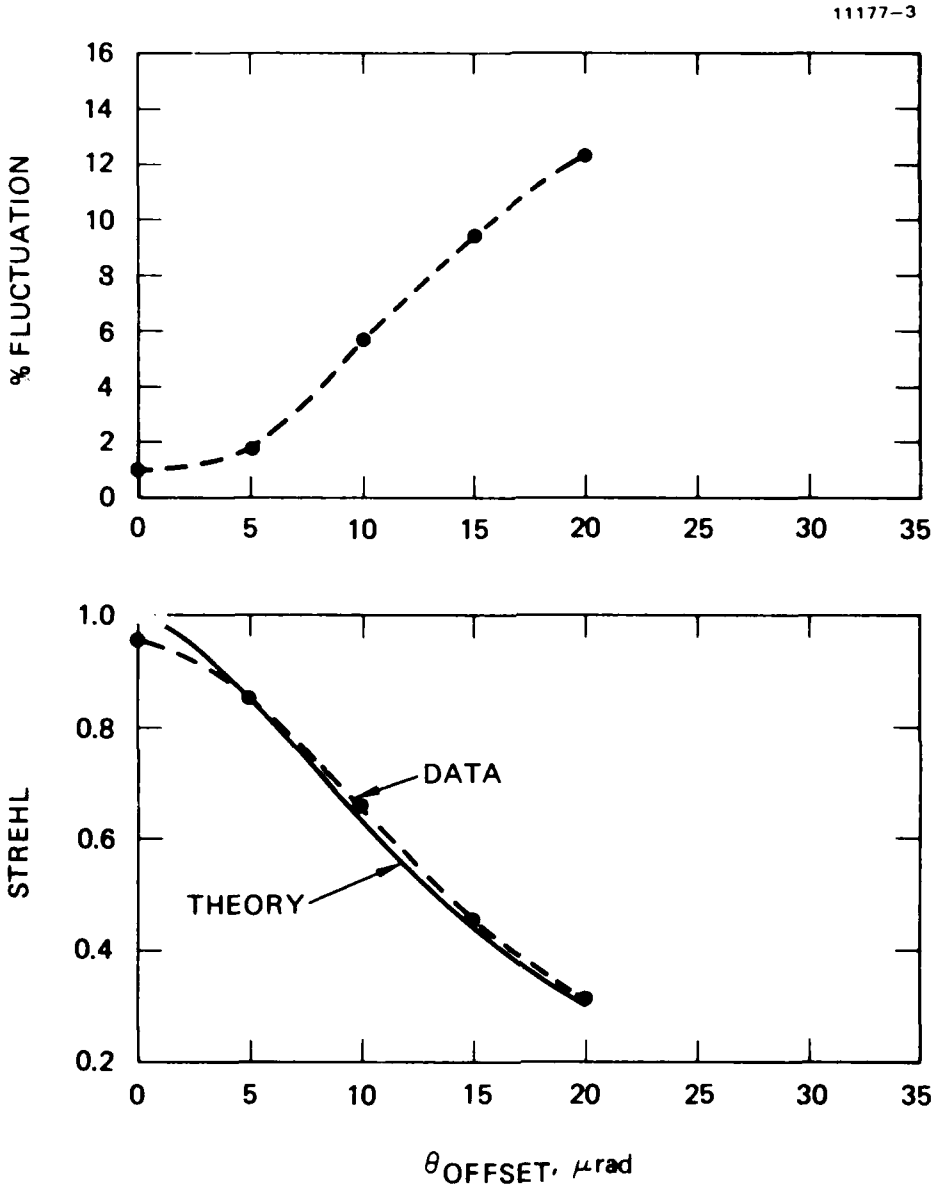

Figure 16. Anisoplanatism for daytime propagation along a zenith path.

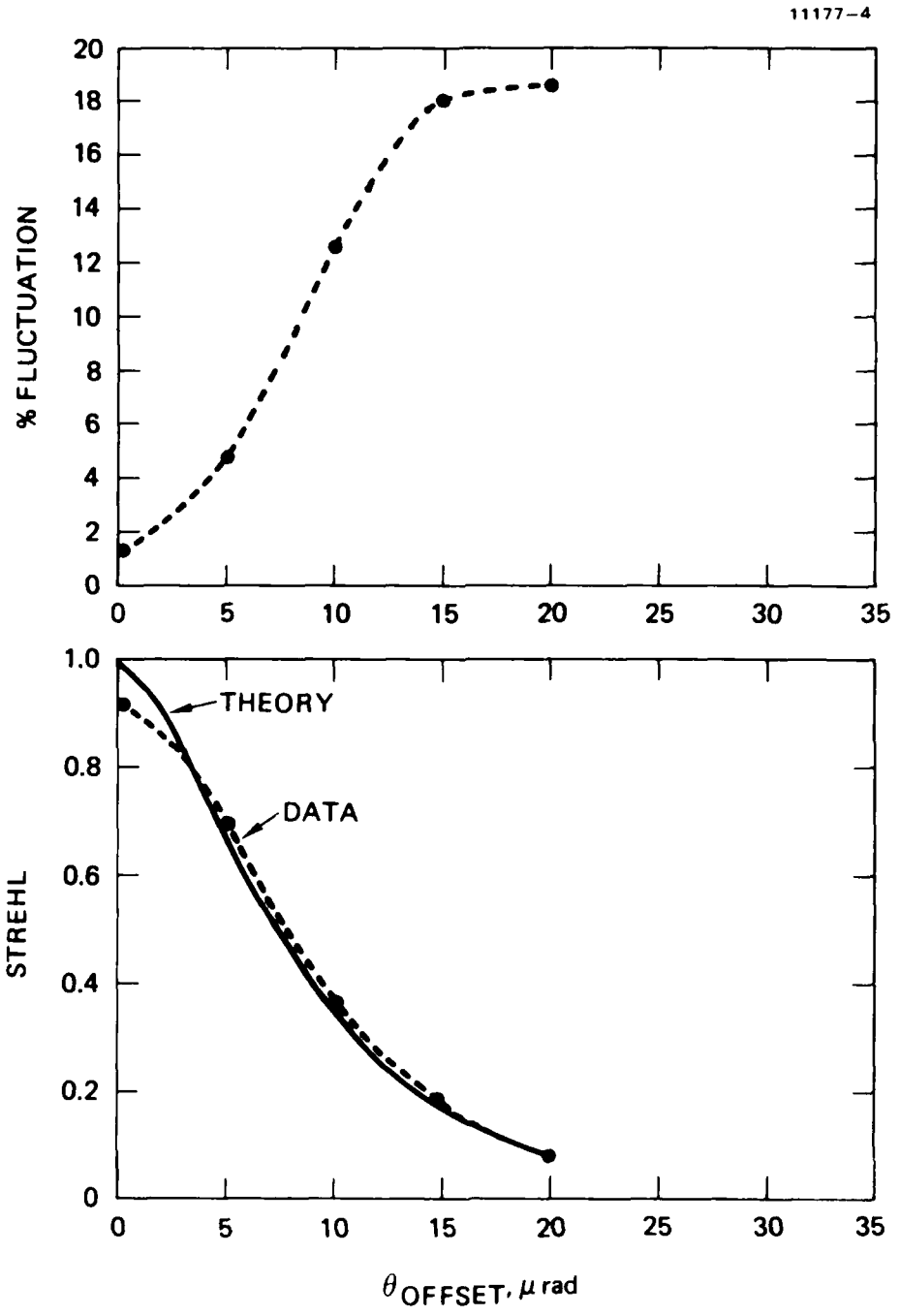

Figure 17. Anisoplanatism for daytime propagation along a slant path at 45° to the zenith.

computer results at zero offset is again a measure of the effect of amplitude scintillation. The fluctuation results illustrate the fact that the level of fluctuation increases as the degree of correction deteriorates. In a positive vein, however, they also indicate that the level of fluctuation is not terribly large even when the Strehl ratio is significantly degraded. Of course, these results say nothing about the probability of deep fades. This type of information requires much more data than were used to obtain the results shown here (recall that each point represents an average over the results of 6 runs).

4.2.3 Finite Temporal Bandwidth Effects

In the anisoplanatic simulations the "perfect" mirror was modeled by calculating the phase of the reference wave with an inverse tangent routine and utilizing the negative of this as the correction phase to be applied to the transmitted wave. Since the phase of the reference wave varies many radians across the transmitter aperture, the wavefront determined by the inverse tangent routine has many two-pi jumps (a jump occurs each time the absolute value of the phase exceeds pi radians). These jumps do not cause problems in the anisoplanatic simulations since they are automatically removed when the transmitter field is evaluated. The same is not true in the simulations performed to explore the effects of finite temporal bandwidth, "perfect" mirror systems. In these simulations

we had to develop a perfect mirror model that does not exhibit the two-pi discontinuities because such jumps do not yield a two-pi jump at the output of a finite temporal bandwidth servo. Instead, two-pi jumps produce nonphysical discontinuities in the phase function. The required "perfect" mirror model was obtained with a routine that calculates phase differences between adjacent mesh points via an inverse tangent routine, and then processes the differences to obtain a smooth phase function. The use of the inverse tangent does not lead to two-pi jumps in this case because the absolute value of the phase differences between adjacent mesh points is always less than pi radians.

Greenwood has derived the following theoretical relation for the effect of servo bandwidth (BW) on the Strehl ratio[18]

$$\text{Strehl Ratio} = \exp(-(2.7\ f_o/BW)^{5/3}), \quad (9)$$

where f_o is a characteristic frequency related to the atmospheric wind velocity and structure constant profiles by

$$f_o = (.0196\ k^2 \int_0^L dz\ C_N^2\ v^{5/3})^{3/5}. \quad (10)$$

The factor 2.7 in Eq. (9) applies to a servo having an RC filter type of response (as does the servo we modeled). As was true in the case of the theoretical predictions for the effects of finite spatial bandwidth and anisoplanatism, the above Strehl ratio relation can be derived entirely on the basis of geometrical optics (although Greenwood did not use geometrical optics to derive his result).

The comparison between the computer simulation results and the theory discussed above is shown in Figure 18. These results apply to nighttime propagation along a zenith path. The characteristic frequency f_o defined above is 5.7 Hz in this case. It should be noted that f_o scales directly with the velocity profile, i.e., increasing the velocities by a multiplicative factor increases f_o by the same factor. Thus, although it might be argued that the velocity profile used in these simulations was too benign, we can easily scale the results to other profiles. Two sets of points are shown in Figure 18, one set corresponding to the original computer results and another set obtained from the original results by dividing by the Strehl ratio at infinite bandwidth (to remove the effects of amplitude scintillation). The agreement between the computer and theoretical results is again quite good. It is interesting

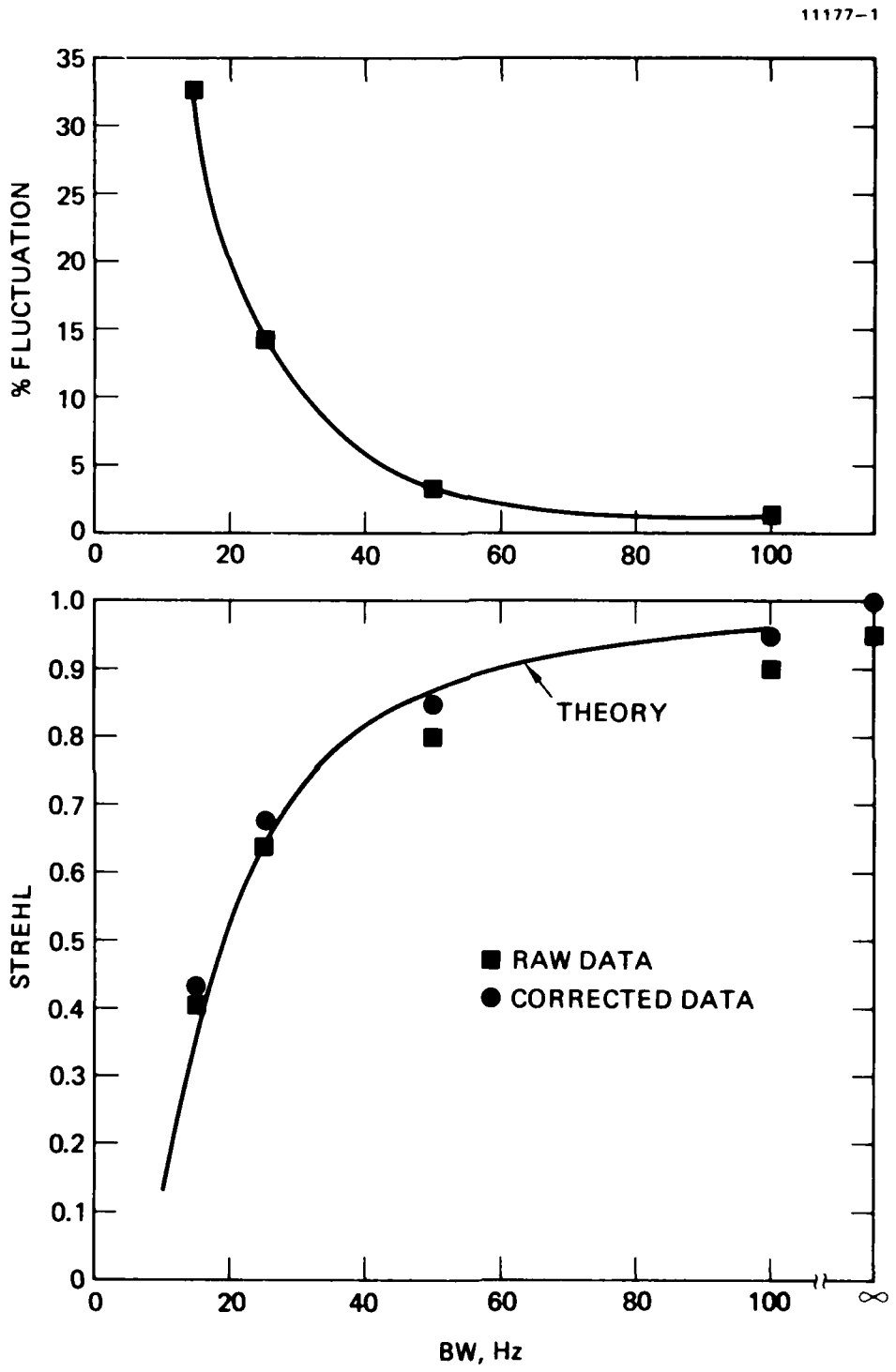

Figure 18. Average Strehl ratio versus temporal bandwidth.

to note that the fluctuation level obtained in these simulations is almost twice as large as that observed in the simulations of the anisoplanatic effects.

Based on these results, it appears that a servo bandwidth in the range from 100 to 300 Hz should be adequate for the SLC Uplink system ... the higher estimate applying to a case in which the wind velocities were three times as large as those used in the simulations.

4.2.4 Noise Effects

The effect of sensor noise is modeled as discussed in Section 2.2. It was assumed in these simulations that the wavefront sensor is a shearing interferometer with a shear distance equal to .4 times the sub-aperture size. Independent samples of gaussian noise are added to the sine and cosine of the phase differences obtained from the wavefront sensor. The rms value of these noise samples was set equal to $1/SNR_i$ where the parameter SNR_i is the instantaneous signal-to-noise ratio of the measurement. The equivalent signal-to-noise ratio of the servo is 2.53 times as large as the instantaneous value by virtue of the fact that it integrates over the individual time samples, thereby reducing the sample noise variance. This can be shown by noting that the servo output $g_o(t)$ resulting from an input signal $g_i(t)$ is

$$g_o(t) = (1/t_o) \int_{-\infty}^{t} dt' \exp(-(t-t')/t_o)\, g_i(t'), \quad (11)$$

where t_o is related to the bandwidth (BW) of the servo by

$$t_o = 1/(2\pi\, BW). \quad (12)$$

The input function corresponding to the discrete data samples used in the simulation is an infinite series of delta functions, i.e.,

$$g_i(t) = \sum (1 + \delta_m)\ \delta(t-t_m), \quad (13)$$

where δ_m is the noise in the m^{th} sample and t_m is time at which the m^{th} datat sample is introduced. Assuming that the data samples are spaced in time by Δt seconds, we find that the servo output is

$$g_o(t) = 1/(1 - \exp(-\Delta t/t_o)) + \sum \delta_m \exp(-m\Delta t/t_o). \quad (14)$$

The first term in Eq. (14) is the noise-free signal and the second is the noise that results from the measurement errors. The net signal-to-noise ratio is obtained by taking the ratio of the signal to the rms noise. This yields

$$SNR = SNR_i(1 - \exp(-2\Delta t/t_o))^{1/2}/(1 - \exp(-\Delta t/t_o)). \quad 15)$$

The time between data samples in the modeling is Δt = .05/BW. With this information, evaluation of Eq. (15) yields the relation mentioned above, viz.

$$SNR = 2.53\ SNR_i. \quad (16)$$

We did not use a perfect mirror in the noise simulations because of the inherent inseparability of the noise and finite actuator problems. The noise introduced in the determination of the actuator positions from the phase-difference measurements depends on the number of actuators. For example, Hudgin[12] has derived the following relation that applies to a shearing interferometer wavefront sensor utilizing the optimal estimation procedure implemented in our software (see Section 2.2).

$$\sigma_\phi^2 = \sigma_{\Delta\phi}^2(.561 + .103\ln(N_{act}^{1/2})), \quad (17)$$

where $\sigma_{\Delta\phi}^2$ is the variance in the phase-difference measurements, which is related to the instantaneous signal-to-noise ratio defined above by

$$\sigma_{\Delta\phi}^2 = 1.2\ [(d/s)/(2.53\ SNR_i)]^2. \quad (18)$$

The factor 1.2 in Eq. (18) has been introduced to account

for the fact that the variance of the noise obtained from the inverse tangent relation used to simulate the operation of the phase-difference sensor is about 20% higher than the internal noise level (this was determined separately by a series of computer "experiments" in which the noise level of the output from the inverse tangent was determined as a function of the input noise level). It was assumed in the simulations that the ratio of the shear distance s to the sub-apertize size d is .4; i.e., the factor d/s in Eq. (18) is 2.5 .

The results obtained in the noise simulations are shown in Figure 19. These results apply to an adaptive-optics system having a 133 actuator deformable mirror and infinite temporal bandwidth (actually, the temporal bandwidth was large compared with the rate at which the atmosphere changes, but finite). The propagation was along a slant path 45° to the zenith having a Miller-Zieske daytime structure constant profile. Two sets of results are shown: (1) the original results which include finite actuator effects as well as noise effects; and (2) results in which the finite actuator (and scintillation) effects have been removed approximately by dividing by the Strehl ratio obtained with an infinite signal-to-noise ratio. Removal of the finite actuator effects in the manner indicated above is probably accurate since the noise and spatial frequency errors are only weakly dependent (in contrast, to the

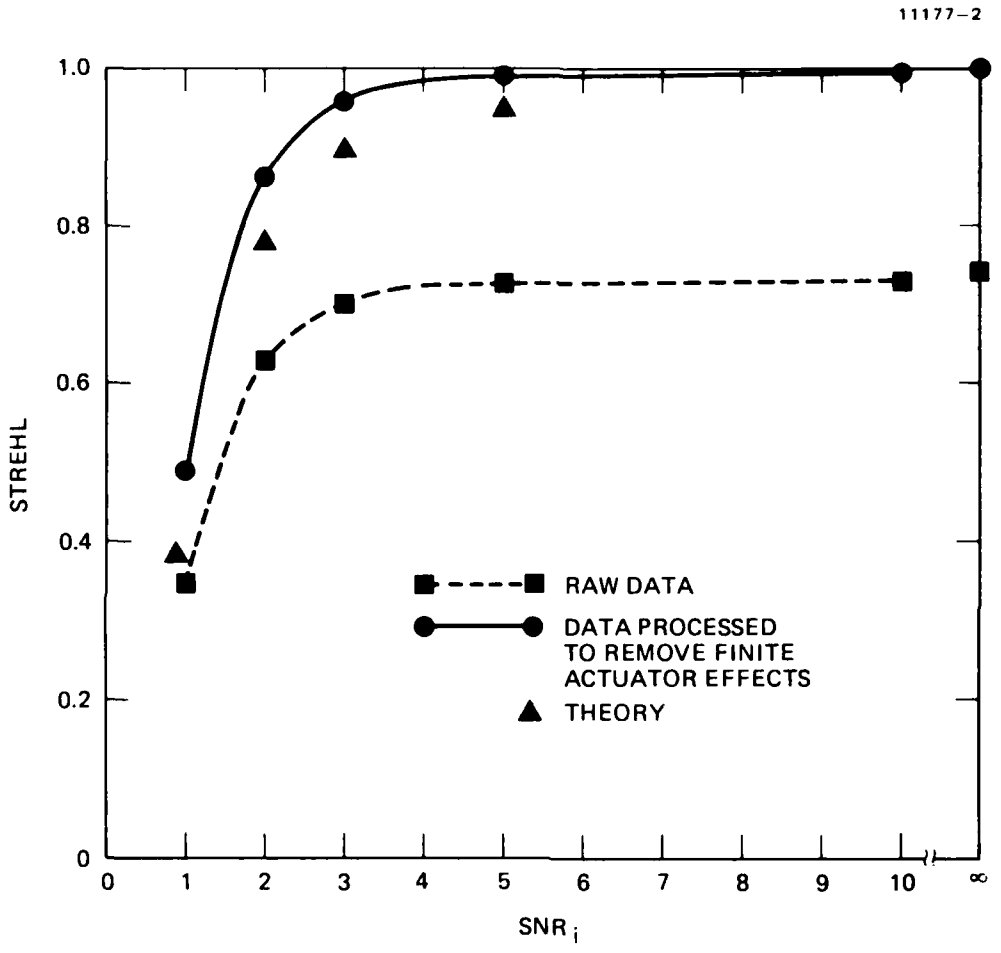

Figure 19. Average Strehl ratio versus sensor signal-to-noise ratio.

dependencies that exist among the errors due to finite spatial bandwidth, finite temporal bandwidth, and anisoplanatism). The agreement between the corrected results and the predictions of the theoretical relation in Eq. (17) is reasonably good, as indicated in the figure.

4.3 Combined Effects of the Errors

Simulation results pertaining to the combined effects of the errors were obtained in two different situations. First, we explored the combined effects of finite actuator and anisoplanatic errors in an adaptive-optics system having infinite temporal bandwidth and signal-to-noise ratio. In addition to being considerably cheaper to simulate since the infinite temporal bandwidth simulations do not require that the propagation information be updated every servo time increment, these simulations provide considerable insight into the nature of the dependency effects. After having completed these simulations we performed a limited set of runs in which all four errors were present. We were primarily concerned in all of these studies with the comparison of the Strehl ratios obtained in the presence of the combined effects with the predictions of the simple theories in which the Strehl ratios corresponding to the separate effects are multiplied to obtain the overall Strehl ratio. The results of our simulations are discussed in the following paragraphs.

4.3.1 Finite Spatial Bandwidth and Anisoplanatism

The results obtained for the combined effects of finite spatial bandwidth and anisoplanatism are given in Figure 20. These results apply to daytime propagation along a zenith path offset 20 μrad. from the point-ahead direction. The adaptive-optics system used in these simulations had infinite temporal bandwidth and signal-to-noise ratio. Simulations were performed for systems having from 64 to 346 actuators. The corresponding range in the ratio of the inter-actuator spacing d to the phase coherence length r_o (=5 cm.) is $2.2 > d/r_o > 1$, as indicated in the figure. Note that the Strehl ratios obtained in the simulations are 50% to 100% larger than the predictions of the simple theory. The size of the discrepancy increased as the spatial bandwidth of the mirror was reduced. This is consistent with the fact that a finite spatial bandwidth mirror does not introduce structure in the phase correction unless it can be resolved by the mirror actuators. Thus, the anisoplanatic errors contributed by spatial frequencies above the cutoff frequency of the mirror are not introduced by the adaptive-optics system and it is not appropriate to include these errors in the Strehl ratio calculation (as the simple theories implicity do). Of course, if the small scale atmospheric structure did not contribute significantly to the anisoplanatic effect, then the error dependence between anisoplanatic and finite actuator effects would be

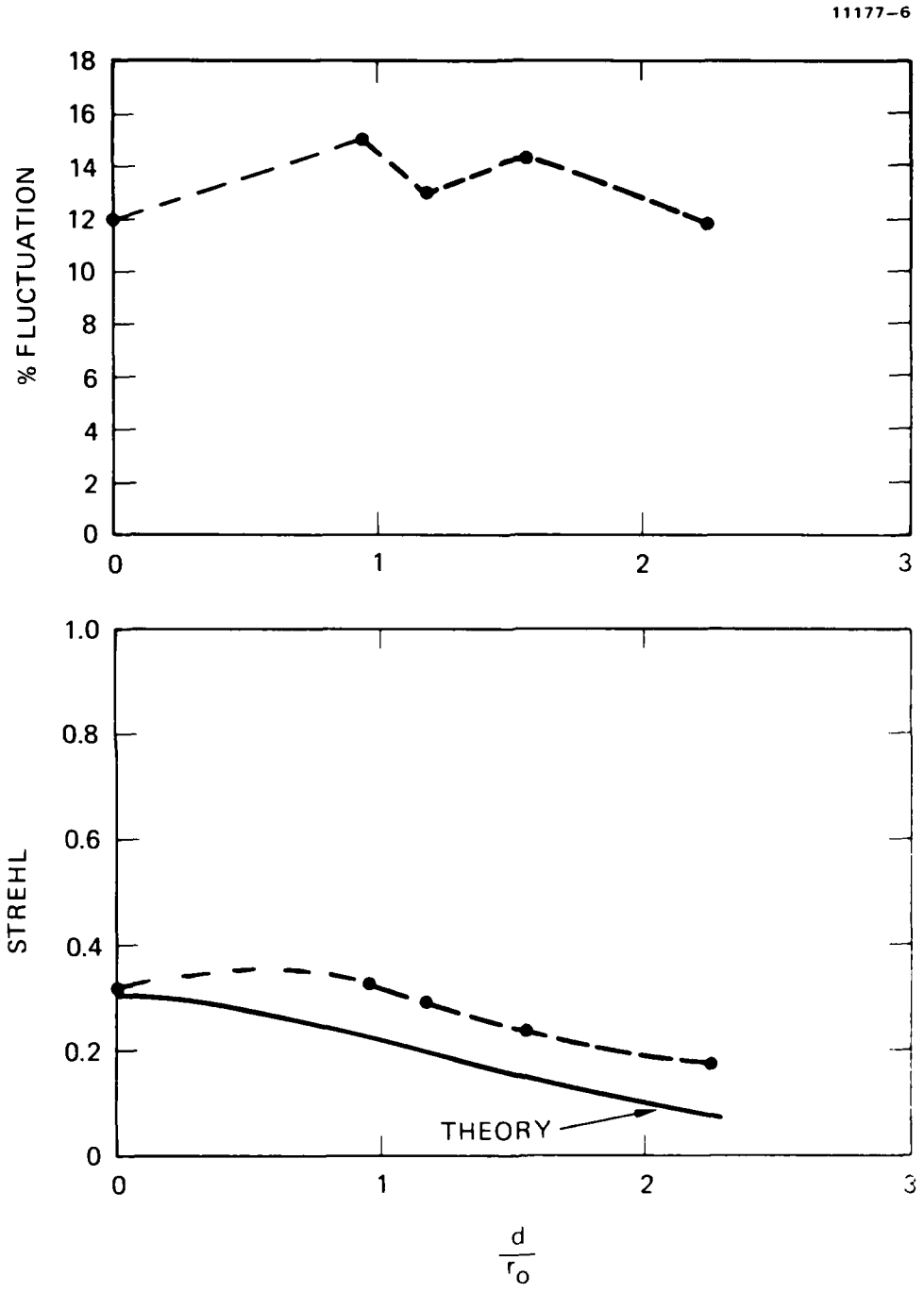

Figure 20. Combined effects of finite spatial bandwidth and anisoplanatism.

reduced. The results shown here and those discussed in Section 4.3.3 below indicate, however, that the anisoplanatic effect depends on spatial frequencies well above the cutoff of the mirrors used in the simulations. It is apparent that anything that limits the spatial frequency response of the adaptive-optics system, even indirectly, will tend to reduce the anisoplanatic effect; e.g., the magnitude of the anisoplanatic effect is dependent on the temporal frequency response of the system because the high spatial frequency wavefront errors generally have high temporal frequency.

4.3.2 Combined Effect of All Errors

We performed only a limited number of simulations in which all four error sources were included. This was necessitated by the lack of sufficient time and computer money to do a more complete study. All of the combined effects simulations were performed with a 256 x 256 propagation mesh and required that the propagation data be updated every servo time increment. Typically, it cost $100 to $140 to make a run long enough that the servo had converged and the results were representative of the steady servo peformance. As mentioned earlier, the average Strehl ratio was caculated by summing the results from 6 runs made with different atmospheric realizations. As a result of the limited number of runs that it was possible to make, we decided to concentrate on cases for which the results might

have some residual practical value to the SLC Uplink program in addition to providing an indication of the importance of the error dependency effects. We chose to simulate three different adaptive-optics systems which illustrate the impact of anisoplanatism on the degree of correction obtainable. In these simulations we utilized a canonical adaptive-optics system having a 1 meter transmit-receive mirror, a deformable corrector mirror having 346 actuators, a 100 Hz servo bandwidth, and a servo signal-to-noise ratio of 7.5. Based on the previous simulation results and the predictions of the simple theories, we expected that such a system would yield nearly diffraction-limited compensation in the absence of anisoplanatism. Results were obtained for systems in which the path of the reference wave was offset from the point-ahead direction by 20, 5, and 0 μrad. (20 μrad. corresponding to a system for which the reference beacon is located on the relay mirror satellite; 5 μrad. to a system for which the station-keep accuracy of the beacon satellite is 5 μrad.; and 0 μrad. to a system having a perfectly positioned beacon satellite).

The results of the combined effects simulations are given in Table I. In the case in which the offset was 20 μrad., the Strehl ratio obtained from the computer simulation was 50% higher than that predicted by theory.

TABLE I. Average Strehl Ratio Including the Combined Effects of All Four Errors

11504-1

θ_{OFFSET}	$SR_{COMPUTER}$	SR_{THEORY}	% FLUCTUATION
20	0.2842	0.1865	21.7
5	0.6126	0.5179	5.8
0	0.6784	0.6104	3.7

This is about the same discrepancy that was obtained in the case discussed above in which the temporal bandwidth and noise errors were zero. This implies that the 100 Hz bandwidth and the signal-to-noise ratio of 7.5 used in the program are sufficiently high that the mirror spatial frequency was the principal source of mirror dependency. Of course, had we simulated a system having substantially lower temporal bandwidth, the discrepancy between the simulation results and the theoretical results would undoubtedly have been larger. In the case in which the offset was 5 μrad., the Strehl ratio obtained from the simulation was 20% higher than predicted by theory, and at zero offset it was 10% higher. The 10% discrepancy obtained at zero offset is indicative of the dependency of the spatial and temporal frequency errors associated with the canonical adaptive-optics system used in these simulations.

It should also be noted again that the magnitude of the fluctuations in target irradiance depends on the fidelity of the correction. In addition to yielding a lower Strehl ratio, an increase in the residual errors leads to an increase in the fluctuation of the irradiance at the relay mirror.

4.3.3 Effect of Translating the Measured Phase Profile

We performed a very limited number of runs in which the phase correction was translated a small distance in the direction opposite to the motion of the relay satellite. It is apparent, on the basis of very simple reasoning having to do with the possibility of reducing the net absolute displacement of the paths taken by the reference and the transmitted waves, that such translations may reduce the magnitude of the anisoplanatic effects. We found that such translations do, in fact, lead to a significant reduction in the anisoplanatic effect if properly chosen. For example, we were able to increase the Strehl ratio obtained for a 20 μrad. offset from the point-ahead direction almost 40% by using this technique. Unfortunately, the practical significance of this result is questionable since it was obtained for an otherwise perfect system. The translation required to yield the increased Strehl ratio was only ? cm . This indicates that the improvement was associated with very small scale errors and thus would undoubtedly not occur for an adaptive system having finite spatial and temporal bandwidth.

V. OPTIMAL ESTIMATION APPLIED TO THE ANISOPLANATIC PROBLEM

It is apparent from what has been said up to this point that it does not necessarily follow that the Strehl ratio at the relay mirror of a SLC Uplink system will increase as the spatial and temporal frequency capabilities of the adaptive-optics system are increased. There are cases in which the best policy may be to use a less capable system. This is illustrated by the results shown in Figure 20, in which we note that the Strehl ratio obtained with a mirror having an inter-actuator spacing equal to the phase coherence length is higher than that obtained with a perfect mirror. In fact, if we do not confine ourselves to the SLC Uplink scenario in which the maximum offset from the point ahead direction is 20 μrad., there are situations in which the best policy is to not use adaptive optics at all. Optimal estimation techniques provide a means of determining the optimal correction policy based on the correlation properties of the phase distortions introduced on the paths taken by the reference and transmitted waves. Hanson[4] has derived an optimal estimation procedure based on the processing successive time samples of the reference wave phase. Unfortunately, this approach will not work for the SLC Uplink system since it is based on the assumption that there is a one-to-one relation between the time and angular

dependence of the wavefront errors. This is not true unless the dominate source of time dependence is associated with the motion of the relay mirror; as it would be, for example, if the relay were located on a satellite in a low altitude orbit rather than a synchronous orbit. We have developed an alternative optimal estimation procedure that does not rely on this assumption. Instead, it utilizes instantaneous phase information available from the measurements made with the shearing interferometer phase difference sensor. This technique is discussed in Section 5.1.

The degree to which the effects of anisoplanatism can be mitigated by optimal estimation depends on the magnitude of the angular offset from the point-ahead direction, the signal-to-noise ratio, and the spatial and temporal bandwidth of the adaptive-optics system. These considerations, which apply to the type of optimal estimation technique developed by Hanson as well as the one discussed in Section 5.1, are discussed in Sections 5.2 and 5.3.

5.1 Optimal Estimation Based on Sub-Aperture Measurements

A set of noisy phase-difference measurements obtained from a shearing interferometer wavefront sensor can be processed to yield an optimal estimate of the phase differences appropriate to propagation along an angularly

displaced path. To derive the relation between the measured and optimal values of the phase differences, we assume that the phase-difference estimates for the displaced path can be expressed as a weighted linear sum of the phase-difference measurements obtained from the reference wave. We have

$$\hat{d\phi}(x_j,\Theta) = \sum A_{ji} \tilde{d\phi}(x_i,0), \quad (19)$$

where Θ is the angle between the paths taken by the reference and transmitted waves, M is the number of measurements to be used in the estimate, and $\tilde{d\phi}$ is the i^{th} noisy phase difference

$$\tilde{d\phi}(x_i,0) = d\phi(x_i,0) + n_i. \quad (20)$$

The optimal choice for the coefficients A in Eq. (19) is determined by the requirement that the mean square error in the associated phase-difference estimates be minimized. This yields a set of linear equations that can be solved to obtain the optimal coefficients in terms of the correlation properties of the phase-differences and the noise.

$$A_{ji} \langle d\phi(x_i,0) d\phi(x_m,0) \rangle = \langle d\phi(x_j,\Theta) d\phi(x_m,0) \rangle + \langle n_j n_m \rangle . \quad (21)$$

5.2 Sensitivity to Noise

The degree to which optimal estimation will improve the performance of an adaptive-optics system depends on the magnitude of the point-ahead angle and the wavefront sensor signal-to-noise ratio. It is obvious that the performance degrades as the point-ahead angle is increased since the optimum policy at very large angles is no adaptive-optics correction at all. Similarly, if the phase-difference measurements are too noisy, the optimum policy is again to forget about the correction. In order to obtain a somewhat more quantitative estimate of the importance of these effects, we will consider a relatively simple estimation problem. In this problem, we are simply trying to estimate the value of a random function of time $f(t+\Delta t)$ based on a sequence of noisy measurement $f(t_i)$. As in the case discussed in Section 5.1, we express the estimate f in terms of a weighted sum of the noisy measurements where the weights are determined by minimizing the mean square error incurred in the estimation. Expressing the results of this calculation in matrix notation , we have the relations

$$\hat{f}(t+\Delta t) = B^T F \ , \qquad (22)$$

$$B = [G^T + I\langle n^2 \rangle]^{-1} H \ , \qquad (23)$$

$$\text{residual error} = \langle f^2 \rangle - B^T H \ , \qquad (24)$$

where B is the matrix of optimal coefficients, F is the matrix of the noisy time samples used to form the estimate of $f(t+\Delta t)$, G is the (two-dimensional) matrix of correlations between the noiseless data samples $f(t_i)$, H is the matrix of the correlations between the function $f(t+\Delta t)$ and the noiseless data samples $f(t_i)$, and $\langle n^2 \rangle$ is the mean square value of the noise (which is assumed to be independent from sample to sample).

To illustrate the dependence of the residual error on the magnitude of the noise, we consider a case in which the random function f has a Gaussian correlation function with a correlation distance t_c; i.e.,

$$\langle f(t_1) f(t_2) \rangle = \langle f^2 \rangle \exp[-(t_1-t_2)^2/t_c^2]. \quad (25)$$

Suppose additionally that the data samples are separated in time by $.2t_c$ and that we wish to estimate the value of f at a time $.5t_c$ after the last data sample. Utilizing the result given in Eq. (24) and the correlation information given in Eq. (25), we find that the residual error is related to the signal-to-noise ratio as indicated in Table II. This table summarizes the error obtained for three different cases: (1) with no optimal estimation; (2) for

TABLE II.

Residual Error as a Function of the Noise Level and the Number of Samples Used in the Estimator.

11504–10

$\mathcal{E}/\langle f^2 \rangle$ / $\frac{\langle f^2 \rangle}{\langle n^2 \rangle}$	N = 0	N = 1	N = 2
∞	0.442	0.393	0.145
10	0.542	0.448	0.429
5	0.642	0.494	0.493
1	1.442	0.697	0.659

optimal estimation based on one time sample; and (3) optimal estimation based on two time samples. Note that when the signal-to-noise ratio is infinite, optimal estimation based on two time samples yields a substantially lower residual error than either of the other two procedures. However, this advantage rapidly disappears as the signal-to-noise ratio is reduced. This is apparently due to the fact that the estimation with two (or more) time samples inherently depends on small differences in the data, which are readily corrupted by noise. On the other hand, the performance of the estimator that uses only one time sample is not very good either. This is due to the fact that we chose the "point-ahead" time to be a substantial fraction (.5) of the time t_c, and it illustrates the fact that the performance of the estimator depends on how far in advance you are trying to estimate. The calculations of Hanson support this conclusion. He has shown that a 25 % reduction in the mean square phase error associated with the anisoplanatic effect is obtained with a two-point estimator when the angular offset is 5 μrad. whereas it is less than 10% when the offset is 50 μrad.. His results neglect the effect of noise and thus give an upper bound on the expected improvement.

5.3 Sensitivity to System Spatial and Temporal Frequency Response

Another important consideration pertinent to the question of the reduction of the effects of anisoplanatism via optimal estimation is the effect of the spatial and temporal frequency response of the adaptive-optics system. We have shown that the magnitude of the anisoplanatic errors depends on the spatial and temporal frequency response of the system. The simulations indicate that the anisoplanatic errors are quite sensitive to the small scale phase variations. Moreover, calculations such as those performed by Valley and Wandzura[19] indicate that the low-order aberrations such as tilt, focus, coma, astigmatism, etc. associated with the atmospheric phase error are correlated over angles much larger than the angle at which significant anisoplanatic effects are observed. This implies that the effect is due to the higher-order aberrations associated with the small scale structure of the phase error.

The above considerations strongly suggest that the reduction in anisoplanatic errors realized with optimal estimation techniques will depend on the spatial and temporal frequency response of the adaptive-optics system. Ideally, such effects should be included in the formulation of the optimal estimation procedure.

VI. CONCLUSIONS AND RECOMMENDATIONS

The computer simulations have shown that error dependency effects can significantly effect the Strehl ratio obtained with a phase-conjugate adaptive-optics system. The predictions of the simple theories, which are based on an assumed independence of the errors due to finite spatial bandwidth, finite temporal bandwidth, and anisoplanatism, are overly pessimistic. The magnitude of the errors caused by this assumption depends on the magnitude of the individual errors. The largest discrepancies occur when the individual errors are large; e.g., when the errors due to anisoplanatism are large. In the case where the reference beacon is located 20 μrad. from the point ahead direction, as would be true if the beacon was located on the relay satellite,we found that the Strehl ratio resulting from the combined effects of these errors was 50% to 100% higher than predicted by theory. Much more modest error is incurred when the individual errors are smaller. For example, the discrepancy between the simple theories and the computer results was only 10% in a case where the anisoplanatic error was zero and the errors due to finite spatial and temporal bandwidth were individually small.

As expected, there was no evidence that the errors due to noise were correlated in any direct way with the other errors (there is a small correlation introduced via the deformable mirror response but this does not appear to be important).

In addition to providing information regarding the average Strehl ratio, the computer simulation results also provide valuable information pertaining to the fluctuation of the compensated field at the relay mirror. We found that the degree of fluctuation depends on the fidelity of the correction. The fluctuation level increases with decreasing Strehl ratio; i.e., as the size of the residual errors increases. Without correction, the irradiance at the relay mirror fluctuates more than 100% about the mean and suffers frequent deep fades. The computer results indicate that the residual fluctuation with adaptive optics will be between 2% and 20% depending on the fidelity of the correction. We did not obtain enough data to determine quantitatively the probability of deep fades, but the results obtained suggest that the likelihood of having a really deep fade is extremely small. It would be worthwhile, however, to perform additional simulations with a simplified propagation model to determine the statistics of the fading more accurately.

We have briefly investigated the effect of optimal estimation on the magnitude of the errors due to anisoplanatism. These studies indicate that the degree of improvement in performance obtained via such techniques will probably be quite small when the effects of noise and the finite spatial and temporal frequency response of the adaptive-optics are taken into account. It also appears that the SLC Uplink system cannot utilize multiple time sample techniques such as that discussed by Hanson[4] since they depend on a high degree of correlation between the variation of the correction phase with time and angle (such as occurs for low altitude satellites where the dominant temporal variation is that due to the slewing motion of the satellite). That is unfortunate since such techniques yield much better performance than those based on single time sampling.

We had originally planned to simulate some of the SLC Uplink adaptive-optics experiments being performed at Lincoln Laboratory. The complications introduced by the necessity to modify the software for operation on the Cray-1 computer, however, consumed the effort that was allotted to these simulations. It would be worthwhile to perform this modeling at a later date since it will provide the first direct comparison between the computer results and a real system.

APPENDIX A

THE EFFECT OF OPTIMAL ESTIMATION ON TURBULENCE COMPENSATION

A.1 Introduction

In this appendix some analytical calculations pertaining to the effect of optimal estimation on the effects of anisoplanatism are discussed. These calculations have been performed along the lines suggested by Valley and Wandzura[15,19] who have determined the angular correlations of atmospheric phase distortion using a modal decomposition approach.

The calculations presented below are for a zonal adaptive-optics system in which the wavefront phase is measured and corrected on an nxn array of sub-apertures, each of which corrects the local tilt. Similar calculations could be performed for modal correction systems; although, at present, there does not seem to be any requirement for these calculations. The calculations proceed as follows. First, the sub-aperture tilt correlation function is obtained as a function of point-ahead angle. Second, the decorrelation is converted into sub-aperture jitter as a function of point-ahead angle; both with and without optimal estimation. The calculations are performed for the

Miller-Zieske nighttime C_N^2 profile defined in Section II of this report. This profile currently appears applicable for blue/green systems at Maui.

A.2 Sub-aperture Tilt Correlation Function

From reference [A2], the sub-aperture correlation functions $C_{\alpha x,\alpha y}$ for the x and y tilts, α_x and α_y, are given by

$$C_{\substack{\alpha x \\ \alpha y}}(\theta/d) = \int_0^\infty dz[A_0(z\theta/d) \pm A_2(z\theta/d)]C_n^2(z)/\int_0^\infty dz(C_n^2(z) \quad (A.1)$$

where the functions $A_{0,2}$ are defined by the integral

$$A_{0,2}(x) = \int_0^\infty du\, u^{-14/3}[J_2(u)]^2 J_{0,2}(2xu). \quad (A.2)$$

Useful approximate analytical fits to A_0 and A_2 are[15]

$$\begin{aligned} A_0(x) &= \exp(-0.5866x^{1.759}) && 0 \le x \le 0.55 \\ &= 0.6656\, x^{-1/3}[1+1/(6^3x^2)] && 0.55 < x \end{aligned} \quad (A.3)$$

$$\begin{aligned} A_2(x) &= \exp(-1.941x^{-0.4602}) && 0 \le x \le 0.625 \\ &= 0.1331\, x^{-1/3}[1-1/(6\Delta^2)] && 0.625 < x \end{aligned} \quad (A.4)$$

Evaluation of Eq (A.1) yields the results shown in the upper curves of Figure A.1. The x tilt decorrelates slightly faster that the y tilt because the point ahead is in the x direction and thus the geometrical overlap of the return and outgoing paths is greater in the y direction. Note that the formulation developed in References 15 and 19 and used here, is purely geometrical and thus ignores the effects of diffraction.

A.2 Sub-aperture Jitter With and Without Optimal Estimation

If one naively uses an estimate of sub-aperture tilt to correct a true tilt a, the sub-aperture jitter (error) is given by

$$\sigma_{\Delta\alpha}^2 = \langle(\alpha-\hat{\alpha})^2\rangle \ .$$

If a and $\hat{a}$ correspond to the same random process displaced by a point-ahead angle θ, then the sub-aperture jitter is given by

$$\sigma_{\Delta\alpha}^2 = 2\sigma_\alpha^2[1-C_\alpha(\theta)] \ .$$

where σ_a is the standard deviation of a and C_a is the correlation function normalized to unity. Note that as θ gets large, C_a goes to zero and $\sigma_{\Delta a}^2 = 2\,\sigma_a^2$. In other words, the "corrected" error variance is twice as large as the uncorrected variance. Optimal estimation is

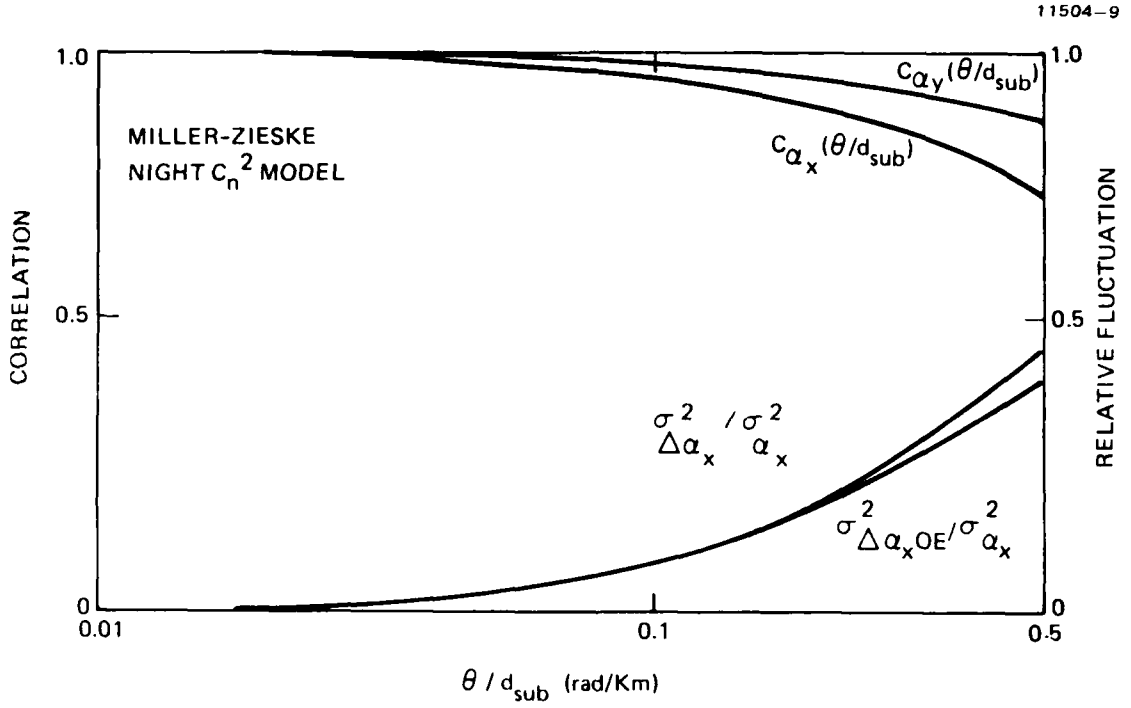

Figure A-1. Correlation and error variance of subaperture tilt measurements.

designed to deal with this undesirable situation.

The optimal estimation value of the sub-aperture tilt estimate, $\hat{a}_{oE}$, is

$$\hat{\alpha}_{oE} = C_{\alpha}(\theta)\hat{\alpha} .$$

In order to obtain this estimate, one requires outside knowledge of the correlation function C_a. The sub-aperture jitter is then given by

$$\sigma^2_{\Delta\alpha oE} = \sigma_{\alpha}{}^2[1-C_{\alpha}{}^2(\theta)] ,$$

which goes to $\sigma_a{}^2$ as θ gets large. The ratio of the variance of the sub-aperture tilt error with and without correction is shown in Figure A.1 both without and with optimal estimation. Note that the advantage produced by optimal estimation is negligible for $\theta/d_{sub} < .1$ rad/km. This is because the correlation function is greater than 0.95 for $\theta/d < .1$. The real advantage with optimal estimation occurs for correlations of .5 or less. But, such correlations imply very poor correction and thus are not relevant to the SLC Uplink application in which good correction is required.

REFERENCES

1. The importance of diffraction effects in the SLC Uplink problem was not clear before the simulation studies were initiated. It was known that dependency effects could be readily included in a geometrical optics formulation but we were not convinced that this was appropriate.

2. R. Pringle, private communication.

3. G. I. Taylor, Proc. Roy. Soc. London, A132, 476, (1938).

4. D. W. Hanson, RADC-TR-81-122, (Aug 81), (A106689)

5. W. P. Brown, Computer Simulation of Adaptive Optical Systems, HRL Final Technical Report on Contract N60921-74-C-0249, (September 1975).

6. Reference will be made available to qualified military and government agencies on request from RADC (OCSE) Griffiss AFB NY 13441.

7. M. Miller and P. Zieske, Turbulence Environment Characterization, RADC-TR-79-131, (Jun 79), (A072379)

8. R. E. Hufnagel, "Variations of Atmospheric Turbulence," OSA Topical Meeting on Optical Propagation Through the Atmosphere, paper WA1, (July 1974).

9. Handbook of Geophysics and Space Environments, ed. by S. L. Valley, McGraw Hill, New York 1965.

10. L. Elterman, Vertical Attenuation Model With Eight Surface Meteorological Ranges 2 to 13 Kilometers, AFCRL-70-0200, AD 707488 (1970).

11. Handbook of Optics, W. G. Driscoll, W. Vaughan eds., McGraw Hill, New York 1978.

12 R. H. Hudgin, J. Opt. Soc. Am., 67, 375 (March 1977).

13. R. J. Roark, Formulas for Stress and Strain, McGraw Hill, New York 1968.

14. W. B. Davenport, Jr., and W. L. Root, Random Signals and Noise, McGraw Hill, New York 1958.

15. G. C. Valley,Appl. Opt.,19,574 (1980).

16. D. L. Fried,Isoplanatism Dependence of a Ground-to-Space Laser Transmitter With Adaptive Optics," Optical Sciences Company Report TR-249 (March 1979).

17. W. P. Brown, unpublished notes.

18. D. P. Greenwood, J. Opt. Soc. Am.,67,390 (March 1977).

19. G. C. Valley and S. M. Wandzura,J. Opt. Soc. Am.,69, 712 (1979).

addresses	number of copies
Capt. Patrick J. Martone RADC/OCSE	15
RADC/TSLD GRIFFISS AFB NY 13441	1
RADC/DAP GRIFFISS AFB NY 13441	2
ADMINISTRATOR DEF TECH INF CTR ATTN: DTIC-DDA CAMERON STA BG 5 ALEXANDRIA VA 22314	12
Hughes Research Laboratories Attn: Dr. Bill Brown 3011 Malibu Canyon Road Malibu, CA 90265	5
Riverside Research Institute 80 West End Ave New York, NY 10023 ATTN: Mr Stephen Aldeman	1
Riverside Research Institute 80 West End Ave New York, NY 10023 ATTN: Dr Marek Elbaum	1
Riverside Research Institute 1701 N Fort Meyer Dr Suite 714 Arlington, VA 22209 ATTN: SLC Library	1

the Optical Sciences Company 1
P.O. Box 446
Placentia, CA 92670
ATTN: Dr David L Fried

MIT/Lincoln Lab 1
P.O. Box 73
Lexington, MA 02173
ATTN: Dr Darryl Greenwood

Scripps Institute of Oceanography 1
University of California, San Diego
P.O. Box 6049
San Diego, CA 92106
ATTN: Mr Ben L McGlamery

Scripps Institute of Oceanography 1
University of California, San Diego
P.O. Box 6049
San Diego, CA 92106
ATTN: Roswell Austin

ORI, Inc 2
1400 Spring Street
Silver Spring, MD 20904
ATTN: C. M. Fowler

W J Schafer Assoc, Inc 2
1901 N Fort Meyer Dr
Suite 800
Arlington, VA 22209
ATTN: Dr William Watt

W J Schafer Associates, Inc 3
1261 Prospect St, Suite 9
P.O. Box 800
La Jolla, CA 92038
ATTN: Dr Gary M Lee

Booz, Allen, & Hamilton 1
4330 East West Hwy
Bethesda, MD 20014
ATTN: Dr Allen Darling

Jet Propulsion Laboratory 1
4800 Oak Grove Drive
Pasadena, CA 91103
ATTN: Mr B. Breshears

Mitre Corporation 1
c/o Naval Ocean Systems Center
San Diego, CA 92152
ATTN: Dr James A Giarati

Adaptive Optics Associates 1
2336 Mass Ave
Cambridge, MA 02140
ATTN: Dr Julius Feinleib

Itek Corporation 2
10 Maguire Road
Lexington, MA 02173
ATTN: Mr Al McGovern

Itek Corporation 1
10 Maguire Road
Lexington, MA 02173
ATTN: Dr L Soloman

Itek Corporation 1
10 Maguire Road
Lexington, MA 02173
ATTN: Mr Ralph Aldrich

TRW 5
Defense & Space Systems Group
One Space Park, R3/2182
Redondo Beach, CA 90278
ATTN: Mr Harold Koletsky

TRW 2
One Space Park
R5/1011
Redondo Beach, CA 90278
ATTN: Mr A. Fiul

Eastman Kodak Company 1
Kodak Apparatus
901 Elmgrove Road
Rochester, NY 14650
ATTN: T. C. Fitzsimmons

Hughes Aircraft Company — 5
Electro-Optical Engineering Division
Centinela & Teale Streets
Culver City, CA 90230
ATTN: Dr C. Chi Bldg 6, MS 6-D137

Hughes Research Laboratory — 2
3011 Malibu Canyon Road
Malibu, CA 90265
ATTN: Dr C. Giuliano

Lockheed Missile Space Corporation — 2
Palo Alto Research Labs
3251 Hanover St
Palo Alto, CA 94304
ATTN: Ms Louise Decker

Rockwell International Corporation — 2
Rocketdyne Division
6633 Canoga Ave
Canoga Park, CA 91304
ATTN: Dr Ken Kissell (FA-36)

Science Applications, Inc — 1
803 W Broad St
Suite 600
Falls Church, VA 22046
ATTN: Dr Emmanuel Goldstein

Environmental Research Institute of Michigan — 1
P.O. Box 8618
Ann Arbor, MI 48107
ATTN: Dr Stanley Robinson

Environmental Research Institute of Michigan — 1
P.O. Box 8618
Ann Arbor, MI 48107
ATTN: Dr J.R. Fienup

DARPA/DEO — 1
1400 Wilson Blvd
Arlington, VA 22209
ATTN: LCDR William Wright

DARPA/IPTO
1400 Wilson Blvd
Arlington, VA 22209
ATTN: Lt Col R. Benedict

1

Naval Electronic Systems Command
PME 106-48
NC 1
Washington DC 20360
ATTN: CDR Donald R McConathy

2

Naval Electronic Systems Command
PME 106-48
NC 1
Washington DC 20360
ATTN: CDR Larry Burgess

2

Naval Electronic Systems Command
PME 106-4A
NC 1
Washington DC 20360
ATTN: Mr Charles Good

1

Naval Electronic Systems Command
PME 106-43
NC 1
Washington DC 20360
ATTN: Mr Stuart J Kearney

1

Naval Electronic Systems Command
PME 110-34
NC 1
Washington DC 20360
ATTN: Mr Wendell Larson

1

Naval Electronic Systems Command
ELEX 611
NC 1
Washington DC 20360
ATTN: Mr Jay McCormick

1

Office of Naval Research
666 Summer Street
Building 114, Section D
Boston, MA 02210
ATTN: Dr M. White

1

Navy Space Systems Activity
P.O. Box 92960
Worldway Postal Center
Los Angeles, CA 90009
ATTN: CDR Lorin Brown

1

Navy Space Systems Activity — 1
P.O. Box 92960
Worldway Postal Center
Los Angeles, CA 90009
ATTN: Hugh Hanson

Naval Ocean Systems Center — 5
San Diego, CA 92152
ATTN: Mr Roy Schindler (8132)

Naval Ocean Systems Center — 1
San Diego, CA 92152
ATTN: LCDR Gary Cooper

Naval Sea Systems Command — 1
NC 1 Rm 11N08
PMS 405-200
Washington DC 20360
ATTN: CDR G P Nanos

RADC (OL-AB) — 1
C/O AVCO Everett Research Labs
P.O. Box 261
Kaneohe, HI 96784
ATTN: Capt Gary Dahlen

TOTAL COPIES REQUIRED 100

MISSION
of
Rome Air Development Center

RADC plans and executes research, development, test and selected acquisition programs in support of Command, Control Communications and Intelligence (C^3I) activities. Technical and engineering support within areas of technical competence is provided to ESD Program Offices (POs) and other ESD elements. The principal technical mission areas are communications, electromagnetic guidance and control, surveillance of ground and aerospace objects, intelligence data collection and handling, information system technology, ionospheric propagation, solid state sciences, microwave physics and electronic reliability, maintainability and compatibility.